Differential *EDS1* requirement for cell death activities of plant TIR-domain proteins

Authors

Oliver Johanndrees*[1], Erin L. Baggs*[2,3], Charles Uhlmann[1], Federica Locci[1], Henriette L. Läßle[1], Katharina Melkonian[1], Kiara Käufer[1], Joram A. Dongus[1], Hirofumi Nakagami[1], Ksenia V. Krasileva[#2,3], Jane E. Parker[#1,4], Dmitry Lapin[#1,5]

1: Department of Plant-Microbe Interactions, Max Planck Institute for Plant Breeding Research, Cologne, Germany

2: Earlham Institute, Norwich Research Park, Norwich, UK

3: Department of Plant and Microbial Biology, University of California Berkeley, Berkeley, California, USA

4: Cluster of Excellence on Plant Sciences (CEPLAS), Cologne - Düsseldorf, Germany

5: Plant-Microbe Interactions, Department of Biology, Utrecht University, Utrecht, The Netherlands

*: these authors contributed equally

#: corresponding authors:

Dmitry Lapin (d.lapin@uu.nl), Jane E. Parker (parker@mpipz.mpg.de), Ksenia V. Krasileva (kseniak@berkeley.edu)

Author contributions

DL, OJ, ELB, KVK, and JEP conceived the project. OJ, ELB, and DL performed sequence and phylogenetic analyses. DL, OJ, KK analyzed RNAseq data. ELB predicted NLRs, OJ, JAD, CU, KM, HN developed CRISPR/Cas9 mutant lines. OJ, HLL, DL, FL, ELB performed immunology assays. OJ, ELB, DL, KVK and JEP analysed the data. OJ, DL

and JEP wrote the manuscript with contributions from ELB and KVK. All authors commented on the manuscript.

One sentence summary

Land plants have evolved four conserved TIR groups

Abstract

Toll/interleukin-1 Receptor (TIR) domains are integral to immune systems across all domains of life. TIRs exist as single-domain and as larger receptor or adaptor proteins. In plants, TIRs constitute N-terminal domains of nucleotide-binding leucine-rich repeat (NLR) immune receptors. Although TIR-NLR and TIR signaling requires the Enhanced disease susceptibility 1 (EDS1) protein family, TIR domains persist in species that have incomplete or no EDS1 members. To assess whether particular TIR groups appear with EDS1, we searched for TIR-EDS1 co-occurrence patterns. Using a large-scale phylogenetic analysis of TIR domains from 39 algae and land plant species, we identify four conserved TIR groups, two of which are TIR-NLRs present in eudicots and two are more widespread. Presence of one TIR-only protein group is highly correlated with EDS1 and members of this group elicit *EDS1*-dependent cell death. By contrast, a more widely represented TIR group of TIR-NB-WD40/TPR (TNP) proteins (formerly called XTNX) has at least one member which can induce *EDS1*-independent cell death. Our data provide a new phylogeny-based plant TIR classification and identify TIR groups that appear to have evolved with and are dependent on *EDS1*, while others have *EDS1*-independent activity.

Introduction

Toll/interleukin-1 Receptor (TIR) domains regulate immune signaling and cell death in bacteria, animals and plants (Leulier & Lemaitre, 2008; Nimma *et al.*, 2017; Bayless & Nishimura, 2020; Ofir *et al.*, 2021). In bacteria, TIR domain proteins likely constitute antiphage defense systems or act as virulence factors (Coronas-Serna *et al.*, 2020; Morehouse *et al.*, 2020; Ofir *et al.*, 2021). In animals, TIRs function as signal transduction

modules within specialized adaptors (e.g. Myeloid differentiation primary response 88 (MyD88)) and in receptor proteins such as Toll-like receptors (TLRs) and Sterile alpha and Toll/interleukin-1 receptor motif-containing protein 1 (SARM1), which sense pathogen-associated molecular patterns (PAMPs) or cell metabolic changes (O'Neill & Bowie, 2007; Figley *et al.*, 2021). In plants, intracellular immune receptors with N-terminal TIR domains have a central domain called nucleotide-binding adaptor shared by APAF-1, certain *R*-gene products, and CED-4 (NBARC or NB-ARC) and C-terminal leucine-rich repeats (LRRs). This receptor class (referred to as TIR-NLR or TNL) detects pathogen virulence factor (effector) activities to induce defenses which often culminate in localized host cell death (Jones *et al.*, 2016). A number of plant truncated TIR-only and TIR-NB proteins also contribute to pathogen detection or defense amplification (Nishimura *et al.*, 2017; Zhang, X *et al.*, 2017b; Bayless & Nishimura, 2020; Tamborski & Krasileva, 2020; Tian *et al.*, 2021). No functional TIR adaptors were found in plants and bacteria to date.

Interactions between activated animal TLRs and TIR adaptor proteins transduce pathogen recognition into defense via protein kinase activation and transcriptional reprogramming (O'Neill & Bowie, 2007; Fields *et al.*, 2019; Clabbers *et al.*, 2021). Importance of these homo- and heterotypic TIR interactions for immune responses is highlighted by the fact that bacterial pathogens in mammals utilize TIR effector hetero-dimerization to disrupt MyD88-mediated TLR signaling (Cirl *et al.*, 2008; Yadav *et al.*, 2010; Nanson *et al.*, 2020). Another TIR mechanism was discovered in human SARM1, in which self-associating TIRs hydrolyze NAD^+ leading to neuronal cell death (Gerdts *et al.*, 2015; Essuman *et al.*, 2017; Horsefield *et al.*, 2019; Sporny *et al.*, 2019). NAD^+ cleavage activity was also found in TIRs of the bacterial antiphage Thoeris system and TIR-STING cyclic dinucleotide receptors (Morehouse *et al.*, 2020; Ofir *et al.*, 2021), bacterial TIR effectors (Coronas-Serna *et al.*, 2020; Eastman *et al.*, 2021), plant TNLs and TIR-only proteins (Horsefield *et al.*, 2019; Wan *et al.*, 2019; Ma *et al.*, 2020). TIR NADase activity and associated host cell death require a conserved catalytic glutamate residue in a pocket formed by the TIR DE interface, BB-loop and the αC-helix in interacting TIRs (Essuman *et al.*, 2017; Essuman *et al.*, 2018; Horsefield *et al.*, 2019; Wan *et al.*, 2019; Ma *et al.*, 2020; Martin *et al.*, 2020; Burdett *et al.*, 2021). Thus, TIRs can regulate host-parasite interactions and cell death via NAD^+ hydrolysis-dependent and independent processes. Many TIR domains are

87 bifunctional enzymes with the capacity for 2',3'-cAMP/cGMP synthetase activity utilizing
88 RNA and DNA substrates in addition to their NADase activity (Yu *et al.*, 2021).

89 Previously, TIRs in prokaryotes and eukaryotes were divided into 37 groups through
90 Bayesian partitioning with pattern selection (BPPS) (Toshchakov & Neuwald, 2020). The
91 majority of plant TIRs were assigned to three plant-specific groups following domain
92 architectures of the full-length proteins, although ~1000 plant TIRs remain unclassified
93 (Toshchakov & Neuwald, 2020). The largest plant-specific group was enriched for TIRs
94 from TNLs, and the two remaining groups included TIR-only proteins and TIRs fused to
95 NBARC-like domains (Toshchakov & Neuwald, 2020). The latter group corresponds to
96 so-called XTNX proteins, where X indicates conserved N-terminal and C-terminal
97 sequences (Meyers *et al.*, 2002; Nandety *et al.*, 2013; Zhang *et al.*, 2016). Because
98 XTNXs contain WD40- and tetratricopeptide-like repeats (TPRs) instead of LRRs (Shao
99 *et al.*, 2019), we call XTNXs from here on TIR-NBARC-like-β-propeller WD40/TPRs
100 (TNPs), to reflect their domain architecture and fitting with existing NLR nomenclature.
101 The BPPS grouping of plant TIRs aligns with earlier studies employing phylogeny-based
102 group assignment of TIRs (Meyers *et al.*, 2002; Nandety *et al.*, 2013).

103 In dicot plants, all tested TIR-only and TNL proteins function via a plant-specific protein
104 family consisting of Enhanced disease susceptibility 1 (EDS1), Phytoalexin-deficient 4
105 (PAD4) and Senescence-associated gene 101 (SAG101) (Lapin *et al.*, 2020; Dongus &
106 Parker, 2021). The EDS1 family proteins contain an N-terminal lipase-like domain and C-
107 terminal α-helical bundle EDS1-PAD4 domain (EP, PFAM: PF18117) with no clear
108 homology outside the EDS1 family (Wagner *et al.*, 2013; Baggs *et al.*, 2020; Lapin *et al.*,
109 2020). EDS1 forms a dimer with either PAD4 or SAG101 to mediate pathogen resistance
110 and cell death triggered by plant TIRs (Wagner *et al.*, 2013; Nishimura *et al.*, 2017;
111 Bhandari *et al.*, 2019; Gantner *et al.*, 2019; Horsefield *et al.*, 2019; Lapin *et al.*, 2019; Wan
112 *et al.*, 2019; Lapin *et al.*, 2020; Sun *et al.*, 2021). By contrast, expression of the human
113 SARM1 TIR domain or *Pseudomonas syringae* HopAM1 TIR effector in wild tobacco
114 (*Nicotiana benthamiana*; *Nb*) triggered *EDS1*-independent cell death (Horsefield *et al.*,
115 2019; Wan *et al.*, 2019; Eastman *et al.*, 2021), suggesting a degree of specificity in
116 translating plant TIR catalytic activity into immune responses via the EDS1 family.
117 Consistent with plant EDS1 family – TIR cofunctions, expanded TNL repertoires correlate

118 with the presence of EP domain sequences in seed plants (Wagner *et al.*, 2013; Lapin *et*
119 *al.*, 2019; Baggs *et al.*, 2020; Liu *et al.*, 2021). However, the existence of TNPs and other
120 TIRs in plant genomes that lack *EDS1* (Meyers *et al.*, 2002; Gao *et al.*, 2018; Toshchakov
121 & Neuwald, 2020) raises the question whether a subset of plant TIRs also function in an
122 *EDS1*-independent manner.

123 Our aim here is to find signatures of EDS1-TIR co-occurrence which could be used to
124 predict EDS1-dependency of distinct TIR domain groups in plants. By phylogeny-based
125 clustering of predicted TIR sequences from 39 species representing diverse groups of
126 green plants, we identify four TIR groups that are shared by at least two plant lineages.
127 Two of these groups match TIRs of the previously identified TNPs and conserved TIR-
128 only proteins (Meyers *et al.*, 2002; Nandety *et al.*, 2013). Two other TIR groups belong to
129 TNLs in Angiosperms. *Nb* tobacco mutants for *TNP*s, encoding the most conserved TIR
130 proteins in plants, behaved like wild type in tested PAMP-triggered and TNL immunity
131 outputs and *TNP* genes were unresponsive in the analyzed immune-related expression
132 assays, suggesting immunity-independent *TNP* functions. We further establish that a TNP
133 from maize elicits *EDS1*-independent cell death in *Nicotiana tabacum* transient expression
134 assays. Conversely, immunity-induced expression of the conserved *TIR-only* genes,
135 dependency of cell death elicited by monocot conserved TIR-only proteins on *EDS1* in
136 *Nb*, and co-occurrence with EDS1/PAD4 in angiosperms suggest the importance of an
137 EDS1/PAD4 – conserved TIR-only signaling node in the immune system of flowering
138 plants. Hence, there appears to be selectivity at the level of EDS1 in plant TIR downstream
139 signaling and cell death activity, which fits patterns of TIR domain phylogeny.

140

141

142 **Results**

143 **Land plants have evolved four conserved TIR groups**

144 To study the distribution of TIRs in plants, we utilized predicted protein sequences from
145 39 species comprising unicellular green algae, non-seed land plants, conifers, and seven
146 clades of flowering plants (*Amborella trichopoda* or *Amborella* hereafter, *Nymphaeales*,
147 *Magnoliids*, *Ceratophyllales*, monocots, superrosids and superasterids) (Supplementary
148 Table 1). In total, 2348 TIRs were predicted using hidden Markov models (HMMs, see

149 Materials and Methods). The number of predicted TIR-containing sequences per plant
150 species ranged from a single protein in *Marchantia polymorpha* (Bowman *et al.*, 2017)
151 and *Selaginella moellendorffii* to 435 and 477 in the Rosid *Eucalyptus grandis* and conifer
152 *Pinus taeda*, respectively. Generally, the highest numbers of predicted TIR-containing
153 proteins were found in eudicots (Supplementary Figure 1a; (Sun *et al.*, 2014; Liu *et al.*,
154 2021)). Analyses of the protein domain composition revealed 1020 TNLs, 401 TN and 572
155 TIR-only architectures (Supplementary Figure 1b-d; note TNPs were excluded from these
156 calculations; (Sun *et al.*, 2014)). As expected, TNLs were missing in monocots and
157 *Erythranthe guttatus* (Shao *et al.*, 2016; Liu *et al.*, 2021) and low TNL numbers were found
158 in two Caryophyllales (*Amaranthus hypochondriacus* and *Beta vulgaris*) as inferred
159 previously (Shao *et al.*, 2016; Lapin *et al.*, 2019; Baggs *et al.*, 2020; Liu *et al.*, 2021).
160 Whereas TNLs were found in 20 of 39 analyzed species, TIR-only proteins (sequences
161 shorter than 400 amino acids and without other predicted PFAM domains) were present
162 in 33 of 39 species, including unicellular green algae and monocots (Supplementary
163 Figure 1d; (Sun *et al.*, 2014; Liu *et al.*, 2021)). Thus, TIR-only is likely the most widely
164 adopted TIR protein architecture across plants.

165 To refine categorization of plant TIRs, we constructed a maximum likelihood (ML)
166 phylogenetic tree for the 2348 TIR sequences (Supplementary Figure 2a, Supplementary
167 Files 1, 2). This analysis revealed four TIR groups shared by several but not all groups of
168 land plants. Algal sequences did not form a monophyletic group and did not fall into the
169 four shared TIR groups. Since algal TIR sequences tended to have long branches, we
170 excluded them from further analysis and repeated the ML tree inference for the remaining
171 2317 TIR sequences (Supplementary Figure 2b, Supplementary Files 3-5). The same four
172 phylogenetically distinct TIR groups appeared as shared by land plant lineages
173 (Supplementary Figure 2b). A large excess of sequences over number of alignment
174 patterns can lead to false phylogenetic inferences. Therefore, we prepared a reduced ML
175 tree for 307 representative TIRs (Figure 1a) selected from the major groups present on
176 the bigger ML tree (Supplementary Figure 2c, Supplementary Files 6, 7). The same four
177 TIR groups were recovered again, despite different alignments and underlying
178 evolutionary models (Figure 1a; BS>90%, SH-aLRT>80), suggesting that categorization
179 of these four TIR groups is consistent across analyses. Since NBARC domain types
180 correlate with NLR groups (Shao *et al.*, 2016; Tamborski & Krasileva, 2020), we tested

181 whether the TIR groups identified here are associated with different NBARC variants. For
182 that, we constructed an ML phylogenetic tree for associated NBARC sequences from full-
183 length TIR-containing sequences used in Figure 1a (Supplementary Figure 3,
184 Supplementary Files 8, 9). NBARCs from sequences within the TIR groups also formed
185 well-supported branches (BS>90%, SH-aLRT>80), suggesting a degree of specificity
186 between conserved TIRs and NBARCs. We conclude that land plants have four
187 phylogenetically distinct TIR groups shared by at least two taxonomic clades.

188

189 **Conserved TIR groups match full-length sequences with different domain**
190 **architectures**

191 Next, we investigated whether full-length proteins within each TIR group have specific
192 domain architectures and how these align with earlier studies. Two conserved TIR groups
193 match two TNL families. One of them is also known as “conserved TNL lineage” or “NLR
194 family 31” in studies deploying NBARC phylogeny and synteny searches (Zhang *et al.*,
195 2016; Liu *et al.*, 2021). We use the term TNL #1 hereafter for this TNL group. The post-
196 LRR C-terminal extension in TNL #1 proteins does not show similarity to other PFAM
197 domains (Supplementary Figure 2b). Since TNL #1 proteins are found in the majority of
198 eudicots and in the monocot-sister magnoliid *Cinnamomum micranthum* (Zhao *et al.*,
199 2021) but not in conifers, *Amborella* or Nymphaeales (Figure 1b), this TIR group likely
200 emerged in mesangiosperms before the split of monocots and dicots and was likely lost
201 in monocots.

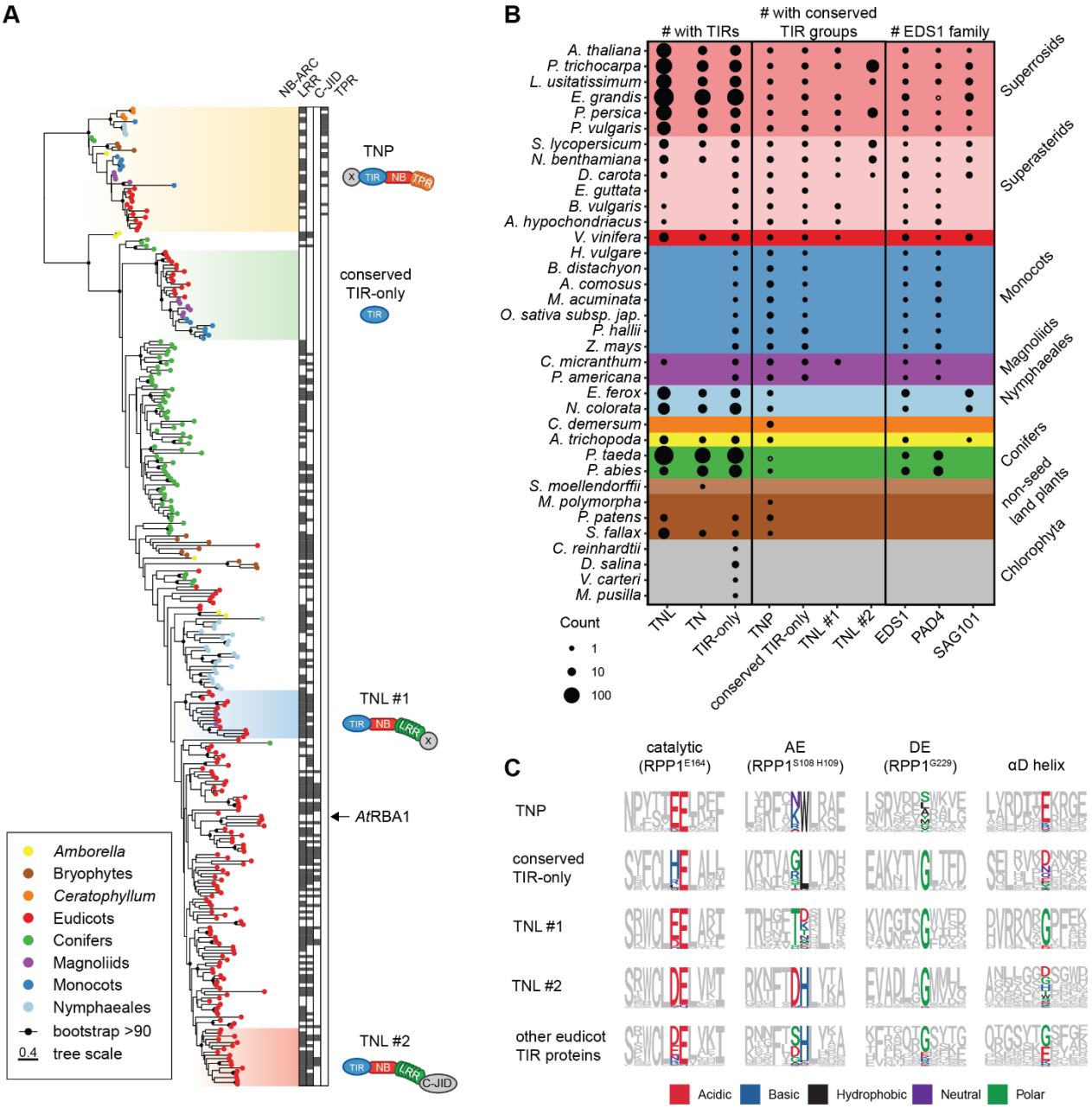

Figure 1 Land plants have four conserved TIR groups.

A ML tree (evolutionary model WAG+F+R7) of 307 predicted TIR domain sequences representing major TIR families across plant species (full 2317 sequence tree in Supplementary Figure 2b). Branches with BS support ≥90 are marked with black dots. Conserved groups with TIRs from more than one species are highlighted with colored boxes and their predominant domain architecture is depicted. Additional domains

210 predicted in the TIR proteins are annotated as black boxes next to each TIR protein (used
211 HMM listed in Supplementary Table 2). Four most conserved TIR domain groups were
212 named after the predominant domain architecture of their full-length proteins. The TIR-
213 only *At*RBA1/*At*TX1 does not belong to conserved TIR-only proteins.

214 **B** Counts of predicted full-length TIR proteins, proteins with conserved TIRs, and
215 EDS1 family predicted in the species analyzed within this study. TNPs are not included in
216 the counts of TNL, TN and TIR-only proteins. TIR-only proteins are defined as sequences
217 shorter than 400 amino acids, without other predicted PFAM domains. Sizes of circles
218 reflect the counts. *Pinus taeda* has one TNP ortholog that was not identified by HMMs,
219 but via reciprocal BLAST. *Eucalyptus grandis* has a fragment of PAD4-like sequence as
220 determined by TBLASTN searches.

221 **C** Comparison of important TIR domain motifs across the four conserved plant TIR
222 groups. Full sets of TIR domains were taken based on phylogeny (tree in Supplementary
223 Figure 2). Sequence motifs were generated for each TIR group to show conservation of
224 the catalytic glutamate, AE and DE interfaces, as well as residues in the αD helix.
225 *At*RPP1^{WsB} TIR domain was taken as reference. Chemical attributes of the important
226 amino acids are annotated in different colors.

227

228 TNLs with the second conserved TIR nested in the NBARC phylogeny-based NLR group
229 called "NLR family 10" in (Zhang *et al.*, 2016). We refer to this NLR family 10-nested TNL
230 group as "TNL #2" (Figure 1a). Our TIR phylogenetic grouping did not find evidence for
231 this conserved TIR in *Arabidopsis thaliana* (*Arabidopsis* from here onwards) and
232 *Amborella*. However, reciprocal BLASTP searches with the respective full-length TNL
233 from domesticated tomato (Solyc01g102920.2.1) suggest that these species have one
234 orthologous sequence each (in *Arabidopsis* - AT5G36930). Because we define sequence
235 groups based on TIR conservation, *Arabidopsis* and *Amborella* TNLs do not fall into the
236 TNL #2 group. In contrast to TNL #1 present in 1-4 copies per genome, the TNL #2 group
237 expanded in some eudicot genomes (e.g., 54 genes in poplar) (Figure 1b, S2b; (Zhang *et*
238 *al.*, 2016)). It comprises ~50% of predicted TNLs in poplar, wild tobacco and tomato. We
239 detected the post-LRR C-terminal jelly-roll/Ig-like domain (C-JID, PFAM: PF20160) in
240 some TNL #2 (Supplementary Figure 2b, Figure 1a; (Van Ghelder & Esmenjaud, 2016;

241 Ma *et al.*, 2020; Martin *et al.*, 2020; Saucet *et al.*, 2021)). Because the C-JID contributes
242 to LRR-specified effector recognition in TNL receptors (Ma *et al.*, 2020; Martin *et al.*,
243 2020), we assume that many TNLs in the TNL #2 group have a role in pathogen detection.

244 The third TIR group (we refer to as conserved TIR-only) corresponds to a small family of
245 ~200 aa-long proteins with a TIR-only architecture and 1-4 gene copies per genome. This
246 group is present in 22 analyzed magnoliids, monocots, and eudicots but absent in
247 conifers, *Amborella* or *Nymphaeales* (Figure 1b), suggesting its emergence in
248 mesangiosperms similar to the TIR of TNL #1. Strikingly, and in contrast to TNL #1,
249 conserved TIR-only proteins are present in monocots. *Arabidopsis* TX3 and TX9 (Nandety
250 *et al.*, 2013) fall into this TIR group. We noticed that the TIR-only effector sensor protein
251 Recognition of HopBA1 (RBA1) does not belong to this conserved TIR-only group (Figure
252 1a; (Nishimura *et al.*, 2017)). Therefore, we conclude that the TIR-protein domain
253 architecture is not a suitable basis for assigning TIR types.

254 The most taxonomically widespread plant TIR-containing proteins are TNPs ((Figure 1b);
255 (Meyers *et al.*, 2002; Zhang, Y-M *et al.*, 2017)). TNPs are almost ubiquitous in analyzed
256 species including the aquatic flowering plant duckweed *Wolffia australiana* with a reduced
257 NLR repertoire (Figure 1b, Supplementary Figure 4, Supplementary Files 10, 11; (Zhang,
258 Y-M *et al.*, 2017; Baggs *et al.*, 2020; Michael *et al.*, 2020; Liu *et al.*, 2021)). The TNP group
259 matches *Arabidopsis* TN17-like and TN21-like sequences (Nandety *et al.*, 2013).
260 Structure-guided comparison with NBARCs from characterized plant NLRs revealed
261 NBARC-characteristic motifs Walker A, RNBS-B, Walker B, RNBS-C, GLPL and MHD,
262 but not the RNSB-B-located TTR/TTE motif (Ma *et al.*, 2020; Martin *et al.*, 2020) in TNP
263 NBARCs (Supplementary Figure 5). We confirmed that the TIR and NBARC-like
264 sequence in TNPs is followed by C-terminal TPRs that are sometimes picked up WD40
265 HMMs (Figure 1a; (Meyers *et al.*, 2002; Nandety *et al.*, 2013; Zhang, Y-M *et al.*, 2017;
266 Shao *et al.*, 2019)). Since a TIR-NBARC-WD40 architecture is present in red algae
267 *Chondrus crispus* (Gao *et al.*, 2018), we tested orthology of TIRs in this algal group to
268 green plant TNPs. Both reciprocal BLAST searches and grouping based on the TIR ML
269 phylogenetic tree (Supplementary Figure 6, Supplementary Files 12, 13) suggest that
270 TIRs from *C. crispus* TIR-NBARC-WD40 sequences are not orthologous to TNP TIRs.

271 Taken together, the four conserved TIR groups matched predicted full-length proteins with
272 different architectures, but these domain architectures are insufficient to define individual
273 TIR groups.

274

275 **Glutamate in the NADase catalytic motif is shared by four conserved TIR groups**

276 We assessed whether key residues critical for plant TIR functions are present in the four
277 conserved TIR groups, utilizing primary sequence and secondary structure-informed
278 alignments. The SH motif is central to an AE dimerization interface in the TIR domains of
279 TNL Resistant to *Pseudomonas syringae* 4 (RPS4) (Williams *et al.*, 2014; Zhang, X *et al.*,
280 2017a). This motif did not show a high level of sequence conservation across the four
281 conserved TIR types (Figure 1c). A glycine residue that is necessary for TIR self-
282 association via a second DE interface and for cell death and NADase activity of
283 *Brachypodium distachyon Bd*TIR and *Arabidopsis* RBA1 TIR-only proteins (Nishimura *et*
284 *al.*, 2017; Zhang, X *et al.*, 2017a; Wan *et al.*, 2019) was conserved in all tested TIR groups
285 except the TNPs (Figure 1c). AlphaFold2 structures of conserved TIR-only proteins from
286 rice and *Arabidopsis* are predicted to differ from known plant TIRs in a poorly structured
287 region in place of the TNL TIR-characteristic αD-helices (see rice TIR-only - grey,
288 *Arabidopsis* – purple in Supplementary Figure 7) (Bernoux *et al.*, 2011). This αD-helical
289 region is important for cell death activities of TNL receptors RPS4 (Sohn *et al.*, 2014) and
290 L6 (Bernoux *et al.*, 2011) and for 2′,3′-cAMP/cGMP synthetase activity found in several
291 plant TIR domains (Yu *et al.*, 2021). The glutamate residue which is indispensable for TIR
292 NADase activity (Essuman *et al.*, 2018; Horsefield *et al.*, 2019; Wan *et al.*, 2019; Ma *et*
293 *al.*, 2020) was present in all four conserved TIRs (Figure 1c), pointing towards a possible
294 NAD^+ hydrolytic activity of these TIR groups.

295

296 **Conserved TIR groups show different co-occurrence patterns with EDS1 family**
297 **members**

298 Since the EDS1 family connects plant TIR activity to resistance and cell death outputs in
299 dicot plants (Lapin *et al.*, 2020), we tested whether the distributions of EDS1 family
300 members and identified conserved TIR groups align across species. We therefore built an

301 ML tree for 200 sequences with an EP domain that uniquely defines the EDS1 family
302 (Supplementary Figure 8, Supplementary files 14 and 15, PFAM PF18117) and inferred
303 numbers of EDS1, PAD4 and SAG101 orthologs per species (Supplementary Table 3,
304 Figure 1b). As expected, EDS1 and PAD4 were present in most seed plants while
305 SAG101 was not detected in conifers, monocots and Caryophyllales (Figure 1b,
306 Supplementary Figure 8, (Lapin *et al.*, 2019; Baggs *et al.*, 2020; Liu *et al.*, 2021). Of the
307 four TIR groups, the conserved TIR-only type showed highest correlation with EDS1 and
308 PAD4 in mesangiosperms (Figure 1b), indicating a possible functionally conserved TIR-
309 only-EDS1/PAD4 signaling module. By contrast, TNPs were present in non-seed land
310 plants and aquatic plants that do not have the *EDS1* family genes (Figure 1b and S4;
311 (Baggs *et al.*, 2020)), pointing to EDS1-independence of TNP activities.

312 The above co-occurrence analyses confirmed that the TNL #1 group has a SAG101-
313 independent distribution in angiosperms (Liu *et al.*, 2021). This prompted us to search for
314 other protein family orthogroups (OGs) that co-occur with TNL #1 and SAG101
315 (Supplementary Figure 9). Using Orthofinder, we built OGs for predicted protein
316 sequences from ten species. Five species (*Oryza sativa, Ananas comosus, Picea abies*,
317 *Erythranthe guttata, Aquilegia coerulea*) lacked SAG101 and TNL #1 (Figure 1b, (Zhang
318 *et al.*, 2016; Liu *et al.*, 2021)). One species (*A. hypochondriacus*) had TNL #1 but no
319 SAG101. Finally, we included four species (*A. thaliana, E. grandis, Populus trichocarpa,*
320 *Solanum lycopersicum*) with SAG101 and TNL #1. We imposed a strict co-occurrence
321 pattern to retain only high confidence candidates. Seven and five OGs followed the
322 SAG101 and TNL #1 distribution, respectively. These findings were refined using
323 reciprocal BLAST searches in genomes of the discriminatory species *Beta vulgaris*
324 (*TNL#1*$^{+}$*/SAG101*$^{-}$*;* (Lapin *et al.*, 2019; Liu *et al.*, 2021)*), Sesamum indicum* and *Striga*
325 *hermonthica* (*TNL#1*$^{-}$/*SAG101*$^{-}$; (Shao *et al.*, 2016; Liu *et al.*, 2021)). After this filter, two
326 OGs showed co-occurrence with SAG101 - *Arabidopsis* hypothetical protein AT5G15190
327 and arabinogalactan proteins AT2G23130/AT4G37450 (AGP17/AGP18) (Supplementary
328 Figure 9). The other two OGs that co-occurred with the conserved angiosperm TNL #1
329 had *Arabidopsis* terpene synthase 4 (TES, AT1G61120) and glutaredoxins ROXY16/17
330 (AT1G03020/AT3G62930) as representatives (Supplementary Figure 9). The functions of
331 these genes in TIR-dependent defense are unknown. Overall, we concluded that

332 conserved TIR groups show different distribution patterns in flowering plants and their co-
333 occurrence with SAG101 is limited.

334

335 **Conserved *TIR-only* genes are transcriptionally induced in immune-triggered**
336 **tissues**

337 The broad species distributions of the four plant TIR groups prompted us to investigate
338 their patterns of gene expression across species. Public RNAseq data for seven plant
339 species including *Arabidopsis thaliana*, *Nicotiana benthamiana*, *Hordeum vulgare,* and
340 *Marchantia polymorpha* were used (Figure 2a, Supplementary Figure 10). The samples
341 originated from infected or immunity-triggered tissues as well as mock-treated or
342 untreated control samples. Relative transcript abundance of *TNP* genes was generally
343 unresponsive to the treatments in dicots and *Marchantia*, but it was elevated in several
344 monocot expression datasets. *TNLs* from the TNL #1 and TNL #2 groups were induced
345 in pathogen-infected *Nb* samples (Supplementary Figure 10). Most strikingly, the
346 conserved *TIR-only* genes were either not detected or expressed at a very low level in
347 non-stimulated tissues but displayed induction in multiple immunity-triggered samples in
348 both monocot and dicot species (Figure 2a, Supplementary Figure 10). To explore further
349 defense-related expression control of *TIR-only* genes, we analyzed time series RNAseq
350 data for *Arabidopsis* with activated bacterial PAMP- or effector-triggered immune signaling
351 (PTI and ETI; Figure 2b, (Saile *et al.*, 2020)). Infiltration of the PTI-eliciting non-pathogenic
352 *Pseudomonas fluorescens Pf*0-1 weakly induced the conserved *Arabidopsis TIR-only*
353 gene *AtTX3*. Higher levels of *AtTX3* expression were detected in samples with *Pf*0-1
354 delivering effectors recognized by NLRs (Figure 2b, (Saile *et al.*, 2020)). Taken together,
355 these observations suggest that expression of the conserved *TIR-onl*y genes is
356 responsive to immunity triggers.

357

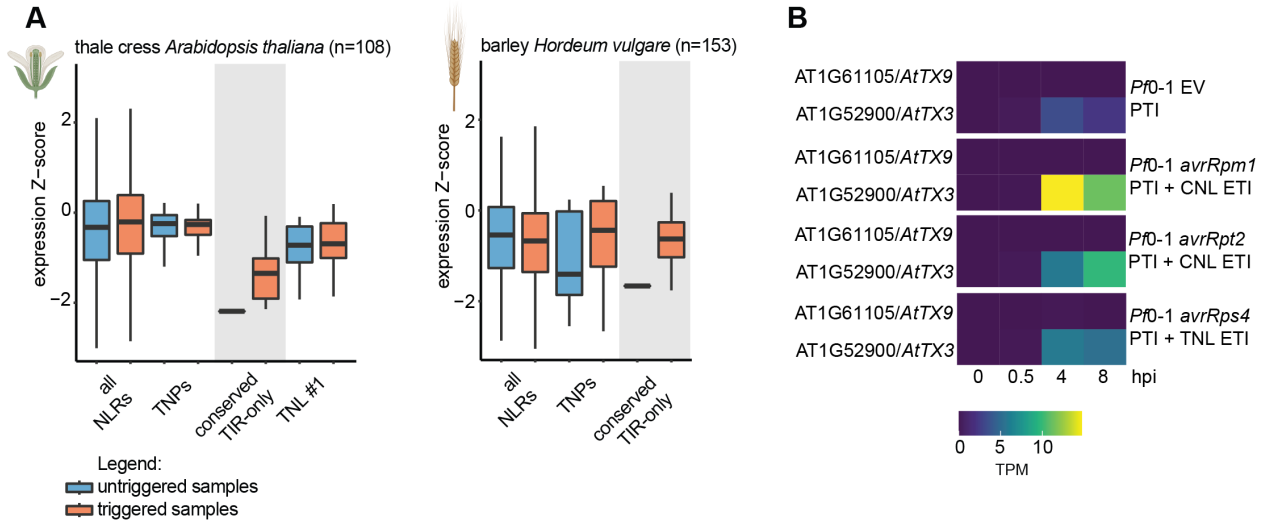

Figure 2 Expression of conserved *TIR-only* genes is upregulated during immune signaling.

A Comparison of untriggered and immune-triggered expression of *NLRs* and genes corresponding to conserved *TIR* groups in *Arabidopsis thaliana* and *Hordeum vulgare*. Data were taken from publicly available RNAseq experiments including immune-triggered and infected samples. Created with elements from BioRender.com.

B Heatmaps showing expression of conserved *TIR-only* genes in PTI and ETI trigger combinations in *Arabidopsis*. Expression data were taken from (Saile *et al.*, 2020). Triggers include *Pseudomonas fluorescens Pf*0-1 empty vector (EV) for PTI trigger, *Pf*0-1 *avrRpm1*, *Pf*0-1 *avrRpm1* for PTI + CNL ETI and *Pf*0-1 *avrRps4* for PTI + TNL trigger. TPM = transcript per million.

Monocot conserved TIR-only induce *EDS1*-dependent cell death in *N. benthamiana*

Since the conserved TIR-only proteins co-occur with EDS1 and PAD4 (Figure 1b), we investigated if they trigger *EDS1*-dependent cell death similar to *B. distachyon* conserved TIR-only (*Bd*TIR) (Wan *et al.*, 2019). For this, we cloned monocot *TIR*-only genes from rice (*Os*TIR, Os07G0566800) and barley (*Hv*TIR, HORVU2Hr1G039670) and expressed them as C-terminal mYFP fusions in *Nb* leaves using *Agrobacterium*-mediated transient

378 expression assays (Figure 3a). Co-expression of TNL Recognition of *Peronospora*
379 *parasitica* 1 (RPP1^{WsB}) with its matching effector ATR1^{Emoy2} as a positive control
380 (Krasileva *et al.*, 2010; Ma *et al.*, 2020) resulted in cell death visible as leaf tissue collapse
381 at 3 days post infiltration (dpi) (Figure 3a). mYFP as a negative control did not produce
382 visible cell death symptoms (Figure 3a). Leaf areas expressing rice and barley conserved
383 TIR-only proteins collapsed in *Nb* wild type (WT) at 3 dpi but not in *eds1a* mutant plants
384 (Figure 3a). As the tested monocot TIR-only proteins accumulated in *Nb eds1a* (Figure
385 3b), we concluded that members of this TIR-only group induce *EDS1*-dependent cell
386 death (Wan *et al.*, 2019). The cell death response was fully suppressed in TIR-only mutant
387 variants in which the NADase catalytic glutamate residue was substituted by alanine
388 (*Os*TIR^{E133A} and *Hv*TIR^{E128A}; Figure 3a). Similarly, mutation of a conserved glycine at the
389 DE TIR interface which is important for TIR NADase activity (Horsefield *et al.*, 2019; Wan
390 *et al.*, 2019; Ma *et al.*, 2020) fully (*Os*TIR^{G188R}) or partially (*Hv*TIR^{G183R}), eliminated the cell
391 death response (Figure 3a). All tested TIR-only variants accumulated in *Nb* leaves (Figure
392 3b). These data show that monocot-derived conserved TIR-only proteins induce host cell
393 death dependent on an intact NADase catalytic site, DE interface and *EDS1* signaling.

394

395 **A maize Clade IIa TNP induces *EDS1*-independent cell death in *N. tabacum***

396 TNPs are present in plants regardless of presence of the EDS1 family (Figure 1b,
397 Supplementary Figure 2, Supplementary Figure 4, (Nandety *et al.*, 2013; Zhang, Y-M *et*
398 *al.*, 2017)). We therefore hypothesized that TNPs act *EDS1*-independently. On the ML
399 tree for TNP NBARC-like sequences selected with help of a custom built HMM
400 (Supplementary Files 16-18), three major TNP clades were recovered, with one splitting
401 into two smaller subclades (Figure 3c). Clade I, Clade IIa and Clade IIb match previously
402 described TNP clades (Zhang, Y-M *et al.*, 2017). Expectedly, Clade IIa is missing from
403 eudicots (Figure 3c, (Zhang, Y-M *et al.*, 2017)). All bryophyte TNP sequences formed a
404 separate third clade (Clade III, Figure 3c). We selected representative sequences from
405 the above three TNP clades to test whether they induce cell death: *Arabidopsi*s
406 AT5G56220 and barley HORVU5Hr1G072030 from Clade I, maize GRMZM2G039878
407 from Clade IIa*, Arabidopsis* AT4G23440 and barley HORVU3Hr1G073690 from Clade IIb,
408 and *Marchantia* Mapoly0134s0035 from the bryophyte-specific Clade III (Figure 3c). The

409 C-terminally tagged (maize TNP was 6xHis-3xFLAG (HF)-tagged, others mYFP-tagged)
410 TNPs were expressed in leaves of tobacco *Nicotiana tabacum* (*Nt*) cv. Samsun or a
411 corresponding RNAi:*EDS1* line (Duxbury *et al.*, 2020) using *Agrobacterium*-mediated
412 transient expression assays. We scored cell death visually as collapse of the infiltrated
413 area at 5 dpi, using co-expression of *At*RPP1^{WsB}-mYFP with effector ATR1^{Emoy2} as a
414 positive control for *EDS1*-dependent cell death (Figure 3d). Expression of maize Clade IIa
415 *Zm*TNP (GRMZM2G039878), but not other TNP forms, consistently resulted in cell death
416 which was *EDS1*-independent (Figure 3d). We were unable to detect any of the TNP
417 proteins on immunoblots. To test whether the predicted maize TNP NADase catalytic
418 glutamate, which is conserved across plant TIRs (Figure 1c), is required for cell death, we
419 substituted adjacent glutamate residues E130 or E131 in *Zm*TNP with alanines
420 (*Zm*TNP^{E130A} and *Zm*TNP^{E131A}; Figure 3e). Cell death was abolished for both mutant
421 variants in cv. “Samsun” and “Turk” tobacco *Nt* cultivars. We concluded that *Zm*TNP likely
422 induces *EDS1*-independent cell death via its TIR putative catalytic motif, although we
423 cannot exclude that *Zm*TNP^{E130A} and *Zm*TNP^{E131A} proteins are less stable than cell death-
424 promoting wild-type *Zm*TNP.

425

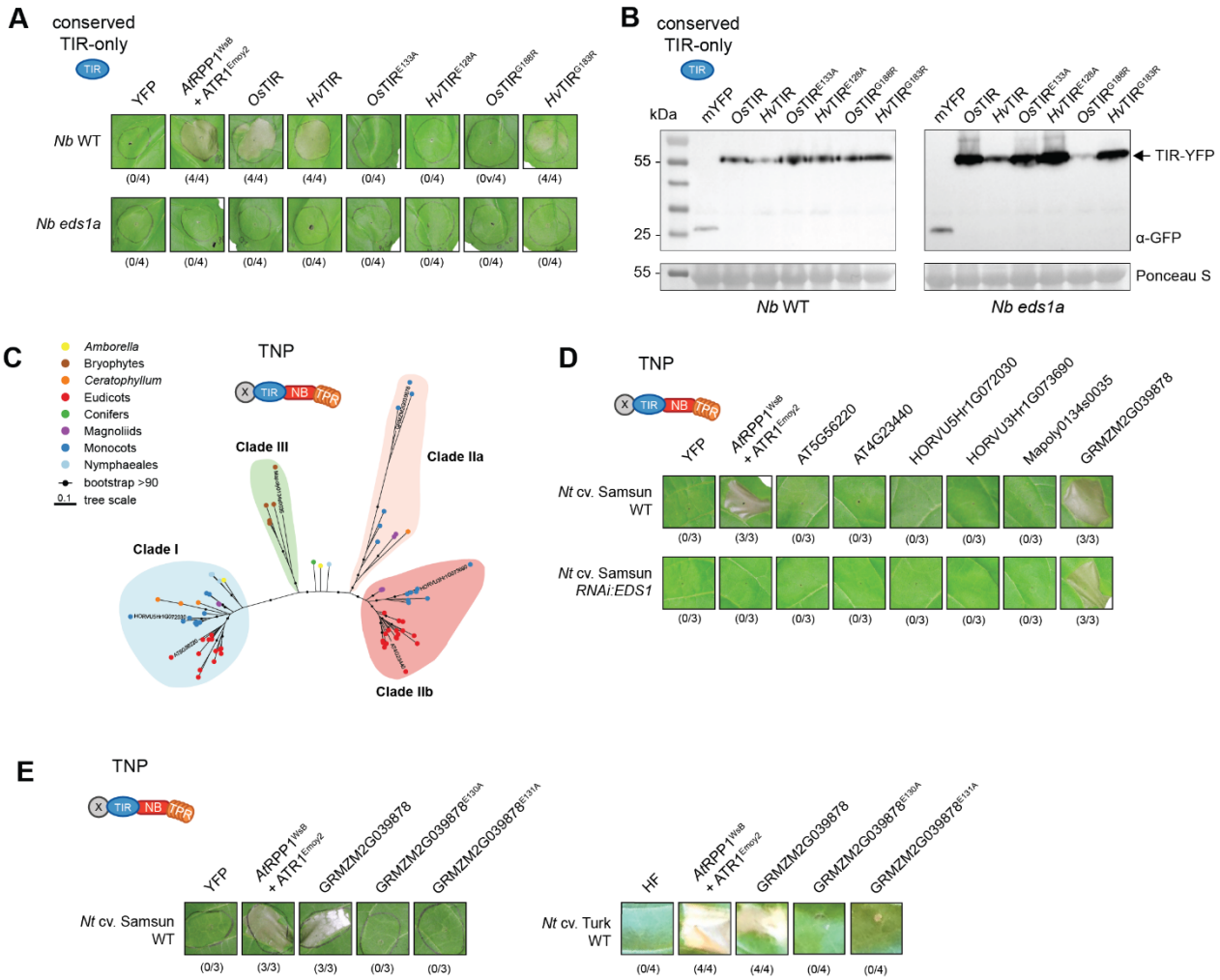

Figure 3 A maize TNP induces *EDS1*-independent cell death in *N. tabacum*.

A Macroscopic cell death symptoms induced by *Agrobacterium*-mediated overexpression of conserved monocot YFP-tagged TIR-only proteins in *Nicotiana benthamiana* (*Nb*) wild type (WT) and the *eds1a* mutant. Pictures were taken three days after agroinfiltrations. Numbers below panels indicate necrotic / total infiltrated spots observed in three independent experiments.

B TIR-only protein accumulation in infiltrated leaves shown in **A** was tested via Western Blot. Expected sizes for YFP-tagged TIR-onlys and free YFP as control are indicated. Ponceau S staining of the membrane served as loading control.

437 **C** ML tree (from IQ-TREE, evolutionary model JTT+G4) of 77 predicted TNP NBARC
438 (Supplementary File 18, E<0.01) domains representing the plant species analyzed withing
439 this study. Branches with BS support ≥90 are marked with black dots. The three conserved
440 TNP clades are highlighted with colored boxes. Clade nomenclature was partly adapted
441 from Zhang *et al.* 2017.

442 **D** Macroscopic cell death symptoms induced by *Agrobacterium*-mediated
443 overexpression of different TNP proteins from four major clades (*Arabidopsis thaliana*,
444 *Hordeum vulgare* and *Marchantia polymorpha* TNPs were YFP-tagged, *Zm*TNP HF-
445 tagged) representing members of clades shown in **C** in *Nicotiana tabacum* (*Nt*) c.v.
446 "Samsun" wild type (WT) and the *RNAi:EDS1* knock-down mutant. Pictures were taken
447 five days after agroinfiltrations. Numbers below panels indicate necrotic / total infiltrated
448 spots observed in three independent experiments.

449 **E** Overexpression of *Zm*TNP WT and mutant variants in the two adjacent putative
450 glutamates (E130, E131) in *Nt* cv. "Samsun" and "Turk" WT. Pictures was taken five days
451 after agroinfiltration and repeated three times with similar results. Numbers below panels
452 indicate necrotic / total infiltrated spots observed in three independent experiments.

453

454 ***Botrytis*-infected *N. benthamiana tnp* mutants develop smaller necrotic lesions**

455 To explore possible TNP functions, we developed two independent CRISPR-Cas9 single
456 and quadruple *tnp* mutants, respectively, in *Marchantia polymorpha* and *Nb*
457 (Supplementary Figure 11). The *TNP*-less plants displayed a similar morphology to wild-
458 type (Figure 4a and 4b). Hence, despite the high conservation and wide distribution in
459 land plants, *TNP* genes do not appear to be essential for growth of tested land plants
460 under laboratory conditions.

461 Since PTI and TNL ETI readouts are well established for *Nb*, we used the two independent
462 *Nb tnp* CRISPR mutant lines to assess whether *TNP* genes influence defense signaling.
463 Reactive oxygen species (ROS) bursts triggered by PAMPs flg22 or chitin were not altered
464 in the *tnp* mutants (Figure 4c,d) indicating that *TNPs* are dispensable for the PAMP
465 perception and induction of immediate downstream ROS burst. Also, the *Nb tnp* mutants
466 allowed wild type (WT)-like growth of virulent *Xanthomonas campestris* pv. *vesicatoria*

467 (*Xcv*) bacteria without a XopQ effector that would otherwise trigger TNL Recognition of
468 XopQ (Roq1) (*Xcv ΔXopQ* Figure 4e). In TNL Roq1 bacterial growth assays, the *tnp*
469 mutants were also indistinguishable from resistant WT plants, although the *eds1a* mutant
470 was fully susceptible to *Xcv* (Figure 4e, (Adlung *et al.*, 2016; Schultink *et al.*, 2017)).
471 Similarly, Roq1 induced cell death was unaffected in the *tnp* mutants after *Agrobacterium*-
472 mediated transient expression of XopQ (Figure 4f), whereas *eds1a* displayed low
473 electrolyte leakage (Figure 4f). Therefore, *TNP*s are dispensable for the tested PTI and
474 ETI outputs in *N. benthamiana*.

475 We analyzed responses of the *Nb tnp* mutants to infection by the necrotrophic fungus
476 *Botrytis cinerea*. Both *tnp* lines developed smaller necrotic lesions 48 h after spore
477 application while the *eds1a* mutant behaved like WT (Figure 4g,h). The phenotypes of WT
478 and *eds1a* compared to *tnp* mutants when challenged with *Botrytis cinerea* suggest that
479 *Nb TNP*s, directly or indirectly, contribute to *B. cinerea* lesion development via an *EDS1*-
480 independent route.

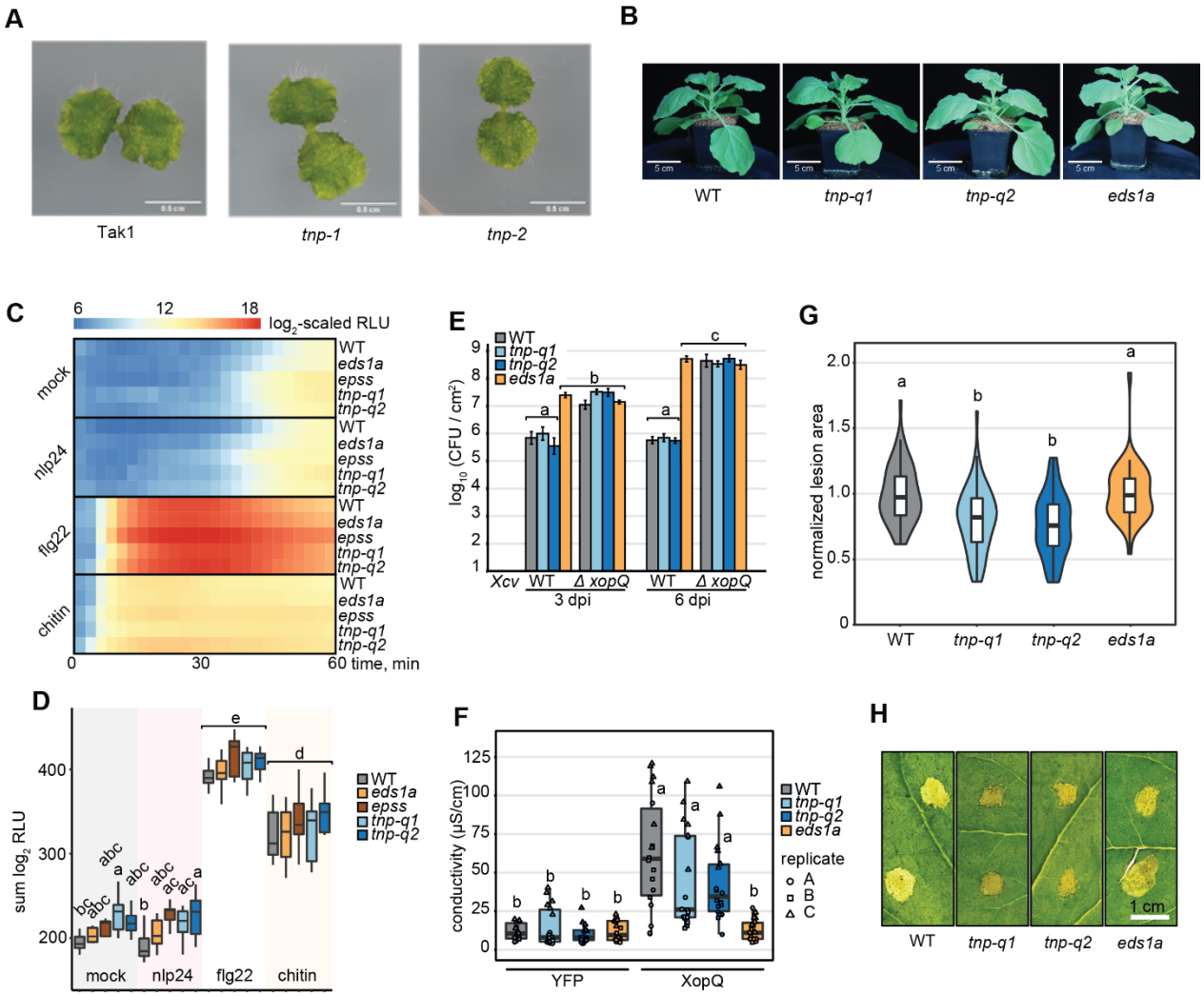

Figure 4 TNPs are not crucial for plant survival but negatively regulate resistance against *Botrytis cinerea* in *N. benthamiana*.

A Macroscopic images of 2-week-old *Marchantia polymorpha* Tak1 WT and two independent *tnp* CRISPR knockout lines. Genomic sequences of the two *tnp* lines are depicted in Supplementary Figure 11.

B Side-view images of 4-week-old *N. benthamiana* WT, two independent *tnp* quadruple CRISPR knockout lines (*tnp-q1*, *tnp-q2*) and the *eds1a* mutant. Plants were grown in long-day (16 h light) conditions. Genomic sequences of the two *tnp* quadruple lines are depicted in Supplementary Figure 11.

492 **C** ROS burst upon several PAMP triggers in *N. benthamiana* WT, *eds1a*, *eds1a pad4*
493 *sag101a sag101b* (*epss*) and *tnp* quadruple mutants (*tnp-q1*, *tnp-q2*). Values are means
494 of log_2-transformed RLU after addition of 2 µM nlp24, 200 nM flg22 or 4 mg/ml chitin and
495 were recorded for 60 min, n = 10-12, from three independent biological replicates.

496 **D** Total ROS produced after 60 min PAMP treatment. Values are sums of log_2-
497 transformed RLU in **C**. Genotype-treatment combinations sharing letters above boxplots
498 do not show statistically significant differences (Tukey HSD, α = 0.05, n = 10-12, from
499 three independent biological replicates).

500 **E** *Xanthomonas campestris* pv. *vesicatoria* (*Xcv*) growth assay in *N. benthamiana*.
501 Plants were syringe-infiltrated with *Xcv* 85-10 (WT) and XopQ-knockout strains (*Δ xopQ*)
502 at OD_{600} = 0.0005. Bacterial titers were determined at three and six days post infiltration
503 (dpi). Genotype-treatment combinations sharing letters above boxplots do not show
504 statistically significant differences (Tukey HSD, α = 0.01, n = 12, from three independent
505 biological replicates).

506 **F** Electrolyte leakage assay as a measure of XopQ-triggered cell death in *N.*
507 *benthamiana* three days after *Agrobacterium* infiltration (OD_{600} = 0.2) to express XopQ-
508 Myc. YFP overexpression was used as negative control. Genotype-treatment
509 combinations sharing letters above boxplots do not show statistically significant
510 differences (Tukey HSD, α = 0.01, n = 18, from three independent biological replicates).

511 **G** Lesion area induced by *Botrytis cinerea* strain B05.10 infection in *N. benthamiana*.
512 Plants were drop-inoculated with spore suspension ($5*10^5$ spores/ml) and lesion areas
513 were measured 48 hours after inoculation. Values shown are lesion areas normalized to
514 WT. Genotypes sharing letters above boxplots do not show statistically significant
515 differences (Tukey HSD, α = 0.01, n = 10-12, from five independent biological replicates).

516 **H** Macroscopic images of *B. cinerea* induced lesions measured in **G**.

517

518

519 **Discussion**

520 TIR signaling domains mediate cell death and immune responses across kingdoms,
521 including plants. Here, we analyzed plant TIR conservation and distribution using newly
522 available genomes from major lineages of land plants and the ML phylogenetic tools
523 (Nguyen *et al.*, 2015; Chernomor *et al.*, 2016) allowing large scale evolutionary analyses.
524 We recovered four interspecific plant TIR groups which so far have no described functions
525 in defense signaling. While two interspecific TIR groups matched TIR-only and TNPs
526 (Meyers *et al.*, 2002; Nandety *et al.*, 2013; Zhang, Y-M *et al.*, 2017; Toshchakov &
527 Neuwald, 2020), two additional TIR groups corresponded to separate angiosperm TNL
528 families. Consistent with differing patterns of co-occurrence with the EDS1 family,
529 conserved TIR-only proteins from monocots and a maize TNP triggered cell death in
530 tobacco, respectively, dependently and independently of *EDS1*. Thus, variation exists in
531 the *EDS1* dependency of plant TIR-promoted cell death.

532 Although TNL NBARCs of land plants are nested within NBARCs of charophytes (Gao *et*
533 *al.*, 2018), none of the four conserved TIR groups included sequences from unicellular
534 chlorophyte algae (Supplementary Figure 2), red algae *Chondrus crispus* and charophyte
535 *Klebsormidium nitens* (Supplementary Figure 6). Also, our reciprocal BLAST searches did
536 not find TNP orthologs in charophytes *K. nitens* and *Chara braunii*. Hence, the conserved
537 TIR groups of land plants likely did not originate in algae. Specifically, our study suggests
538 that TIR groups from conserved TIR-only and TNL groups #1 and #2 have likely emerged
539 in flowering plants. Major TIR groups of animals (TIRs of TLRs, Myd88, SARM1) are
540 present in *Drosophila melanogaster* and *Homo sapiens* separated by ~700 million years
541 (confidence interval 643-850 MY) (O'Neill & Bowie, 2007; Toshchakov & Neuwald, 2020).
542 However, a lack of detectable orthology for three of four TIR groups across non-seed land
543 plants (~500 MY, confidence interval 465-533 MY) (Kumar *et al.*, 2017) suggests that plant
544 and animal TIRs may be evolving under different constraints and selection pressures.

545 We show that the full-length protein domain architecture is insufficient to define TIR
546 groups. Conserved TIR-only proteins form a group that is phylogenetically distinct from
547 TIR-only RBA1 (also known as *At*TX1) and *At*TX12 (Nandety *et al.*, 2013; Nishimura *et*
548 *al.*, 2017) which are closer to the TIRs of TNLs RPS4 and Lazarus 5 (LAZ5)
549 (Supplementary Figure 2). *EDS1*-dependent cell death activity of conserved and

550 RBA1/TX-like TIR-only proteins (Figure 3a; (Nishimura *et al.*, 2017; Horsefield *et al.*, 2019;
551 Wan *et al.*, 2019; Duxbury *et al.*, 2020)), as well as their immunity-related transcriptional
552 induction (Figure 2; (Nandety *et al.*, 2013)), suggest functional convergence of TIR-only
553 groups in plant immunity. Since TIR-only is the most widespread TIR protein architecture
554 in green plants (Supplementary Figure 1; (Sun *et al.*, 2014)), structure-informed
555 comparative analyses of different TIR-only groups will be crucial to understand plant
556 immunity networks.

557 We found differences in copy number of the different TIR group members, with over 50
558 eudicot TNLs #2 present in the poplar genome in contrast to 1-4 gene copies for the other
559 TIR groups. NLRs have among the highest copy number variation in plants (Baggs *et al.*,
560 2017), ranging from 3,400 NLRs in *Triticum aestivum* (Steuernagel *et al.*, 2020) to 1 in
561 *Wolffia australiana* (Michael et al., 2020). High variability in copy number is often
562 associated with the generation of diversity towards a sensor role (Nozawa & Nei, 2008;
563 Kanduri *et al.*, 2013; Prigozhin & Krasileva, 2021), whereas conserved low copy number
564 is a feature of signaling components. Presence of the effector-sensing C-JID domain in
565 multiple eudicot TNLs #2 (Figure 1a, Supplementary Figure 2) further suggests they act
566 as pathogen-sensors. It will be interesting to test if conserved TIR-only proteins act as
567 plant TIR adaptor proteins similar to Myd88 and Myd88 adaptor-like cofunctioning with
568 PAMP-recognizing TLRs (O'Neill & Bowie, 2007; Nanson *et al.*, 2020).

569 The absence of conserved TNLs and TIR-only clades in multiple plant species (Figure 1b)
570 suggests that these TIR protein families are not essential for plant viability. TNPs are
571 almost ubiquitous to land plants (Zhang, Y-M *et al.*, 2017) and we generated CRISPR-
572 Cas9 mutants of all *TNPs* in *M. polymorpha* and *Nb*. Tobacco quadruple *tnp* mutants and
573 the effectively *TIR*-less *M. polymorpha tnp* mutant were viable and had no obvious growth
574 defects under laboratory conditions (Figure 4). Thus, TNPs and other TIR-containing
575 proteins are likely not essential for plant growth in contrast to Toll and TLR signaling in
576 animals (Anthoney *et al.*, 2018), however further research is needed to clarify this.

577 We found that conserved TIR-only from monocots and a *Zm*TNP triggered cell death in
578 tobacco leaves (Figure 3a,c,d) and this likely required a glutamic acid residue in their
579 conserved catalytic motifs (Figure 1c), as observed in plant TIRs (Horsefield *et al.*, 2019;
580 Wan *et al.*, 2019). Notably, expression of *Zm*TNP in *N. tabacum* resulted in an *EDS1*-

581 independent cell death, resembling SARM1 (Horsefield *et al.*, 2019) and HopAM1
582 (Eastman *et al.*, 2021). These findings suggest that plant TIRs have differing enzymatic
583 activities (Horsefield *et al.*, 2019; Wan *et al.*, 2019; Duxbury *et al.*, 2020) selectively
584 promoting EDS1 family signaling. Given that several plant TIRs were reported to have2′,3′-
585 cAMP/cGMP synthetase activity besides being NADases (Yu *et al.*, 2021), it will be
586 interesting to examine the range of enzymatic functions across plant TIR groups and how
587 these affect plant immunity.

588 **Materials and methods**

589

590 **Prediction, alignment and phylogenetic analysis of TIRs and other domains**

591 Proteomes of 39 plant species (Supplementary Table 1) were screened for TIR domains
592 using hmmsearch (HMMER 3.1b2, --incE 0.01) with TIR and TIR-related HMMs from the
593 Pfam database (Supplementary Table 2). Redundant TIR sequences found with different
594 TIR and TIR-like HMMs (overlap >20 aa) were removed. Proteins predicted to contain TIR
595 domains were used to build a multiple sequence alignment (MSA) using the MAFFT
596 algorithm (v7.407, fftns or ginsi, with up to 1000 iterations) (Katoh *et al.*, 2002). The MSA
597 was filtered and columns with more than 40% gaps were removed using the Wasabi MSA
598 browser (http://was.bi/). The remaining sequences were used to build the maximum
599 likelihood phylogenetic trees with IQ-TREE (version 1.6.12, options: -nt AUTO -ntmax 5 -
600 alrt 1000 -bb 1000 -bnni, (Nguyen *et al.*, 2015; Chernomor *et al.*, 2016)). The resulting
601 trees were visualized and annotated using the online phylogenetic tree manager iTOL v5
602 (Letunic & Bork, 2021) or the R package ggtree (Yu, 2020). Sequence data were
603 processed in R with the Biostrings (https://bioconductor.org/packages/Biostrings).
604 Prediction of other domains was performed with hmmsearch (HMMER 3.1b2, --E 0.01) on
605 Pfam A from release 34.0.

606

607 **Presence and absence analysis of proteins consistent with SAG101 and**
608 **conserved angiosperm TNL #1**

609 Orthofinder (v.2.3.11) was run on the following proteomes: P.abies 1.0, Osativa 323 v7.0,
610 Acomosus 321 v3, Acoerulea 322 v3, Ahypochondriacus 459 v2.1, Slycopersicum 514
611 ITAG3.2, Mguttatus 256 v2.0, Athaliana 167 TAIR10, Egrandis 297 v2.0, Ptrichocarpa 533
612 v4.1. The *P.abies* proteome was downloaded from congenie.org, all other proteomes were
613 downloaded as the latest version of primary transcript from the Phytozome database (v12)
614 on March 31 2020. Then, we extracted orthogroups that followed the pattern of presence
615 and absence of interest using the following custom scripts
616 extract_orthogroup_TNL_absent_v2.py and extract_orthogroup_SAG101_absent_v2.py.
617 Scripts and orthofinder output are available on github (https://github.com/krasileva-
618 group/TIR-1_signal_pathway.git). *A. thaliana* genes from each orthogroup were searched

619 using tBLASTn against *S. indicum* (Ensembl Plants), *S. hermonthica* (COGE) and *B.*
620 *vulgaris* (Ensembl Plants). The top hit was then searched with BLASTX or BLASTP (if a
621 gene model was available) back against *A. thaliana* proteome.

622

623 **Generation of expression vectors**

624 *TNP* coding sequences without Stop codons were amplified from cDNA (*Arabidopsis*
625 *thaliana* Col-0, *Hordeum vulgare* cv. Golden Promise, *Oryza sativa* cv. Kitaake,
626 *Marchantia polymorpha* Tak1) using oligos for TOPO or BP cloning (Supplementary Table
627 4). Coding sequences were amplified with Phusion (NEB) or PrimeStar HS (Takara Bio)
628 polymerases and cloned into pENTR/D-TOPO (Thermo Fisher Scientific) or pDONR221
629 vectors and verified by Sanger sequencing. Mutations in the sequences were introduced
630 by side-directed mutagenesis (Supplementary Table 4). Recombination of sequences into
631 pXCSG-GW-mYFP (Witte *et al.*, 2004) expression vector was performed using LR
632 Clonase II enzyme mix (Life Technologies). *ZmTNP* was synthesized by TWIST
633 Bioscience with codon optimization for expression in *Nicotiana benthamiana;* two
634 fragments were required to synthesize *ZmTNP*. The two fragments were ligated during
635 golden gate cloning into pICSL22011 (oligos listed in Supplementary Table 4) using BsaI
636 restriction sites. Vectors were verified by Sanger sequencing. Site directed mutagenesis
637 of *ZmTNP* was carried out using Agilent technologies QuickChange Lightning Site-
638 Directed Mutagenesis Kit (210518) (oligos listed in Supplementary Table 4). Expression
639 vectors harbouring *At*RPP1^{WsB} and ATR1^{Emoy2} were previously published (Ma *et al.*,
640 2020).

641

642 **Transient protein expression and cell death assays in tobacco species**

643 *Agrobacterium tumefaciens* strains GV3101 pMP90RK or pMP90 carrying desired
644 plasmids were infiltrated into *Nicotiana benthamiana or Nicotiana tabacum* leaves at a
645 final OD_{600} of 0.5. For *N. benthamiana* infiltrations, *A. tumefaciens* strain C58C1 pCH32
646 expressing the viral DNA silencing repressor P90 was added (OD_{600} = 0.1). Prior to
647 infiltration using a needle-less syringe, *A. tumefaciens* strains were incubated in induction
648 buffer (10 mM MES pH 5.6, 10 mM $MgCl_2$, 150 nM Acetosyringone) for 1 to 2 h in the dark

649 at room temperature. Protein samples were collected at 2 dpi for Western Blot assays.
650 Macroscopic cell death was recorded using a camera at 3 dpi. For electrolyte leakage
651 assays, six 8 mm leaf disks were harvested for infiltrated leaf parts at 3 dpi and washed
652 in double-distilled water for 30 min. After washing, leaf disks were transferred into 24-well
653 plates, each well filled with 1 ml ddH_2O. Conductivity of the water was then measured
654 using a Horiba Twin ModelB-173 conductometer at 0 and 6 hours.

655

656 **Western blot analysis**

657 To test protein accumulation after *A. tumefaciens* infiltrations in tobacco plants, three 8
658 mm leaf disks were harvested per protein combination at 2 dpi and ground in liquid
659 nitrogen. Ground tissue was dissolved in 8 M Urea buffer, vortexed for 10 min at RT and
660 centrifuged at 16,000 xg for 10 min (Ma *et al.*, 2020). Total protein extracts were resolved
661 on a 10 % SDS-PAGE gel and subsequently transferred onto a nitrocellulose membrane
662 using the wet transfer method. Tagged proteins were detected using primary antibodies
663 (list antibodies) in a 1:5000 dilution (1x TBST-T, 2 % milk (w/v), 0.01 % (w/v) NaAz),
664 followed by incubation with HRP-conjugated secondary antibodies. Signal was detected
665 by incubation of the membrane with Clarity and Clarity Max substrates (BioRad) using a
666 ChemiDoc (BioRad). Membranes were stained with Ponceau S as loading control.

667

668 **ROS burst assays in *N. benthamiana***

669 A ROS burst in response to PAMP elicitors was measured according to (Bisceglia *et al.*,
670 2015). Four-mm leaf discs from 4th or 5th leaves of 5-week-old *Nb* plants were washed in
671 double-distilled (mQ) water for 2h and incubated in 200 µl of mQ water in 96-well plates
672 (Greiner Bio-One, #655075) under aluminum foil overnight. The mQ was then substituted
673 by a solution of L-012 (Merck SML2236, final 180 µM) and horseradish peroxidase (Merck,
674 P8125-5KU, 0.125 units per reaction). Elicitors flg22 (Genscript, RP19986, final 0.2 µM),
675 chitin (from shrimp shells, Merck C7170, resuspended in mQ for 2h and passed through
676 22 µm filter, final 4 mg/ml), and nlp24 (Genscript, synthesized peptide from
677 *Hyaloperonospora arabidopsidis* NLP3 AIMYAWYFPKDSPMLLMGHRHDWE, crude
678 peptide, final 2 µM) were each added to a 250 µl reaction. Luminescence was recorded

679 on a Glomax instrument (Promega) at 2.5 min intervals. Log_2-transformed relative
680 luminescence units were integrated across time points for the statistical analysis (ANOVA,
681 Tukey's HSD test).
682

683 **_Xcv_ infection assays in _N. benthamiana_**

684 *Xanthomonas campestris* pv. *vesicatoria* (*Xcv*) bacteria was infiltrated in four weeks old
685 *N. benthamiana* mutant leaves at a final OD_{600} of 0.0005. The *Xcv* strain carrying XopQ
686 (WT) and one strain lacking XopQ (Δ *xopQ*) were dissolved in 10 mM $MgCl_2$. Bacterial
687 solutions were infiltrated using a needleless syringe. After infiltration, plants were placed
688 in a long-day chamber (16 h light/ 8 h dark at 25°C/23°C). Three 8 mm leaf disks
689 representing technical replicates were collected 0, 3 and 6 dpi to isolate the bacteria and
690 incubated in 1 ml 10 mM $MgCl_2$ supplemented with 0.01 % Silvet for 1h at 28 °C at 600
691 rpm shaking. Dilutions were plated on NYGA plates containing 100 mg/L rifampicin and
692 150 mg/L streptomycin.

693

694 **_Botrytis_ infection assays in _N. benthamiana_**

695 *Botrytis cinerea* strain B05.10 was grown on potato glucose agar (PGA) medium for 20
696 days before spore collection. Leaves from 4/5-week-old soil-grown *Nicotiana*
697 *benthamiana* were drop inoculated by placing 10 µl of a suspension of 5×10^5
698 conidiospores ml^{-1} in potato glucose broth (PGB) medium on each side of the middle vein
699 (4/6 drops per leaf). Infected plants were placed in trays at room temperature in the dark.
700 High humidity was maintained by covering the trays with a plastic lid after pouring a thin
701 layer of warm water. Under these experimental conditions, most inoculations resulted in
702 rapidly expanding water-soaked necrotic lesions of comparable diameter. Lesion areas
703 were measured 48 hours post infection by using ImageJ software.

704

705 **Generation of _M. polymorpha tnp_ CRISPR/Cas9 mutants**

706 Guide RNA design was performed using CRISPR-P 2.0
707 (http://crispr.hzau.edu.cn/CRISPR2/) where the sequence of Mapoly0134s0035 was

708 inputted (guide RNAs are listed in Supplementary Table 4). *Marchantia polymorpha* Tak-
709 1 was transformed as described in (Kubota *et al.*, 2013) with the exception that
710 *Agrobacterium tumefaciens* strain GV3101 pMP90 was employed. Briefly, apical parts of
711 thalli grown on 1/2 Gamborgs B5 medium for 14 days under continuous light were
712 removed using a sterile scalpel and the basal part of each thallus was sliced in 4 parts of
713 equal size. These fragments were then transferred to 1/2 Gamborgs B5 containing 1%
714 sucrose under continuous light for 3 days to induce calli formation before co-culture with
715 *A. tumefaciens*. On the day of co-culture, *A. tumefaciens* grown for 2 days in 5 ml liquid
716 LB with appropriate antibiotics at 28°C and 250 rpm were inoculated in 5 ml liquid M51C
717 containing 100 µM acetosyringone at an estimated OD_{600} of 0.3-0.5 for 2.5 to 6 hours in
718 the same conditions. The regenerated thalli were transferred to sterile flasks containing
719 45 ml liquid M51C and *A. tumefaciens* was added at a final OD_{600} of 0.02 in a final volume
720 of 50 ml of medium with 100 µM acetosyringone. After 3 days of co-culture agitated at 400
721 rpm under continuous light, the thalli fragments were washed 5 times with sterile water
722 and then incubated 30 min at RT in sterile water containing 1 mg/ml cefotaxime to kill
723 bacteria. Finally, plants were transferred to 1/2 Gamborgs B5 containing 100 µg/ml
724 hygromycin and 1 mg/ml cefotaxime and grown under continuous light for 2 to 4 weeks.
725 Successful mutagenesis was validated by PCR amplification (oligos listed in
726 Supplementary Table 4) and subsequent Sanger sequencing. Two independent lines
727 were selected for further experiments.

728

729 **Generation of *N. benthamiana tnp* CRISPR/Cas9 mutants**

730 Guide RNA design was performed using CRISPR-P 2.0
731 (http://crispr.hzau.edu.cn/CRISPR2/) where the four *NbTNP* sequences were inputted
732 (guide RNAs are listed in Supplementary Table 4). *N. benthamiana* WT plants were
733 transformed according to (Ordon *et al.* 2019, dx.doi.org/10.17504/protocols.io.sbaeaie).
734 Successful mutagenesis was validated by PCR amplification (oligos listed in
735 Supplementary Table 4) and subsequent Sanger sequencing. Two homozygous
736 quadruple mutants were selected.

737

738 **Analysis of publicly available immune-related RNAseq datasets**

739 RNAseq data (Supplementary Table 5) were downloaded from Sequence Read Archive
740 with sra toolkit (SRA Toolkit Development Team, https://github.com/ncbi/sra-tools;
741 v.2.10.0). After FastQC quality controls (Andrews, S. 2010; A Quality Control Tool for High
742 Throughput Sequence Data; http://www.bioinformatics.babraham.ac.uk/projects/fastqc/),
743 reads were trimmed with Trimmomatic (v0.38, LEADING:5 TRAILING:5
744 SLIDINGWINDOW:4:15 MAXINFO:50:0.8 MINLEN:36) (Bolger *et al.*, 2014). Transcript
745 abundance was quantified with Salmon (v.1.4.0, --fldMean=150 --fldSD=20 for single-end
746 reads, --validateMappings –gcBias for paired-end reads) (Patro *et al.*, 2017). The tximport
747 library (v 1.22.0) was used to get the gene expression level in transcript-per-million (tpm)
748 units (Soneson *et al.*, 2015). Since RNAseq samples are coming from diverse studies that
749 use different library preparation methods and sequencing platforms, tpm values were
750 standardized per sample and the derived z-scores were used for visualization of the
751 expression levels. Genome versions used as a reference for transcript quantification:
752 *Arabidopsis thaliana* - TAIR10, *Oryza sativa* group *japonica* - IRGSP-1.0, *Hordeum*
753 *vulgare* - IBSCv2, *Zea mays* - B73v4, *Marchantia polymorpha* v3.1, *Nicotiana*
754 *benthamiana* v1.0.1. NLR genes were predicted with NLRannotator
755 (https://github.com/steuernb/NLR-Annotator; (Steuernagel *et al.*, 2020)).

756

757

758 **Supplementary Data**

759 Supplementary Table 1. List of species used in this study

760 Supplementary Table 2. List of HMMs used in this study

761 Supplementary Table 3. Counts of EDS1 family members across species

762 Supplementary Table 4. Oligonucleotides used in this study

763 Supplementary Table 5. List of RNAseq accessions

764

765 Supplementary File 1. Alignment used to produce ML tree in Supplementary Figure 2a

766 Supplementary File 2. ML tree in Supplementary Figure 2a (Newick format)

767 Supplementary File 3. Alignment used to produce ML tree in Supplementary Figure 2b

768 Supplementary File 4. ML tree in Supplementary Figure 2b (Newick format)

769 Supplementary File 5. Protein sequences containing TIR domains in Supplementary
770 Figure 2a

771 Supplementary File 6. Alignment used to produce ML tree in Figure 1a

772 Supplementary File 7. ML tree in Figure 1a (Newick format)

773 Supplementary File 8. Alignment used to produce ML tree in Supplementary Figure 3

774 Supplementary File 9. ML tree in Supplementary Figure 3 (Newick format)

775 Supplementary File 10. Alignment used to produce ML tree in Supplementary Figure 4

776 Supplementary File 11. ML tree in Supplementary Figure 4 (Newick format)

777 Supplementary File 12. Alignment used to produce ML tree in Supplementary Figure 6

778 Supplementary File 13. ML tree in Supplementary Figure 6 (Newick format)

779 Supplementary File 14. Alignment used to produce ML tree in Supplementary Figure 8

780 Supplementary File 15. ML tree in Supplementary Figure 8 (Newick format)

781 Supplementary File 16. Alignment used to produce ML tree in Figure 3c

782 Supplementary File 17. ML tree in Figure 3c (Newick format)

783 Supplementary File 18. Custom Hidden Markov model based on TNP-NBARC

784

785

786 **Supplementary Figure Legends**

787 **Supplementary Figure 1 TIR distribution across 39 plant species.**

788 **A** Total number of TIR domains predicted in plant species representing major algae
789 and land plant taxa.

790 **B** Number of proteins with a TIR-NBARC-LRR (TNL) domain structure.

791 **C** Number of proteins with a TIR-NBARC (TN) domain structure.

792 **D** Number of proteins with a TIR-only architecture (<400 aa long sequences with no
793 other predicted domains).

794

795 **Supplementary Figure 2 Complete TIR phylogeny across tested plant species.**

796 **A** Maximum likelihood (ML) phylogenetic tree (evolutionary model JTT+F+R10) of
797 2348 predicted TIR domain sequences representing major TIR families across 39 plant
798 species (including green algae). Branches with ultrafast bootstrap (BS) support ≥95 are
799 marked with black dots. Conserved groups with TIRs from more than one taxonomic group
800 are highlighted with colored boxes.

801 **B** ML tree (evolutionary model JTT+F+R9) for 2317 predicted TIR domain sequences
802 (same dataset as in A but excluding algal TIRs). Branches with ultrafast BS support ≥95
803 are marked with black dots. Conserved groups with TIRs from more than one species are
804 highlighted with colored boxes.

805 **C** Same tree as in **B** with red triangles marking position of selected TIR sequences
806 used to construct ML tree in Figure 1a.

807

808 **Supplementary Figure 3 Phylogeny of TIR-associated NBARC domains.**

809 ML tree (evolutionary model JTT+F+R5) for 178 NBARC domain sequences predicted as
810 additional domains in the representative TIR protein dataset shown on the ML tree in
811 Figure1A. Branches with ultrafast BS support ≥90 are marked with black dots. Conserved
812 groups with TIRs from more than one species are highlighted with colored boxes.

813

814 **Supplementary Figure 4 TNP tree for aquatic plants.**

815 ML tree (evolutionary model PROTCATJTT, from RAxMLv8.2.9) for 201 proteins
816 containing the NB-ARC-like domain HMM identified by HMMsearch of proteomes. Tree
817 includes species with and without *EDS1*. Branches with BS support ≥90 are marked with
818 black dots. The blue clade indicates TNPs.

819

820 **Supplementary Figure 5 NBARC sequence alignment and motifs.**

821 Amino-acid sequence alignment (from MUSCLE) of NLR proteins NB-ARC domain and
822 TNP protein NB-ARC like domains. Black boxes highlight conserved motifs characterized
823 due to their importance for NLR function. Above the red line are TNP protein sequences
824 and below are TNL. CNL and RNL sequences.

825

826 **Supplementary Figure 6 TIR phylogeny including TIRs from *Chondrus crispus* and**
827 ***Klebsormidium nitens*.**

828 ML tree (evolutionary model WAG+F+R7) for 353 predicted TIR domain sequences (same
829 dataset as in Figure1A but including predicted TIRs from the red algae *Chondrus crispus*
830 and the charophyte *Klebsormidium nitens*). Branches with BS support ≥90 are marked
831 with black dots. Conserved groups with TIRs from more than one species and *Chondrus*-
832 and *Klebsormidium*-specific groups are highlighted with colored boxes.

833

834 **Supplementary Figure 7 Alignment of predicted structures of conserved TIR-only**
835 **structural comparison to TNL TIRs.**

836 Solved structures of the RPS4 (PDB:4c6t, chain B), RPP1 (PDB:7crc, chain C) and L6
837 (PDB:3ozi, chain A). TIR domains were aligned in PyMol (v3.7) to predicted structures of
838 conserved TIR-only proteins from *Arabidopsis* (AT1G52900, AlphaFold2, UniprotID
839 Q9C931, accessed 15 Aug 2021, alphafold.ebi.ac.uk) and rice (Os07G0566800,
840 AlphaFold2, UniprotID Q7XIJ6, accessed 15 Aug 2021, alphafold.ebi.ac.uk). Positions of
841 major TIR-TIR AE and DE self-association interfaces as well as the BB-loop region and
842 catalytic glutamates are highlighted with arrows. αD helical region of conserved TIR-only

843 proteins AT1G52900 and Os07G0566800 is likely less structured compared to RPS4,
844 RPP1 and L6 TIRs.

845

846 **Supplementary Figure 8 EP domain phylogeny to access presence/absence of**
847 **EDS1 components in plant proteomes.**

848 ML tree (evolutionary model JTT+F+R7) for predicted EP domain sequences. Based on
849 phylogeny, numbers of predicted EDS1, PAD4 and SAG101 orthologues were calculated
850 per species. Branches with BS support ≥95 are marked with black dots. Conserved groups
851 with EP domains from EDS1, PAD4 or SAG101 are highlighted with colored boxes.

852

853

854 **Supplementary Figure 9 Presence-absence of TNL #1, SAG101 and orthogroups**
855 **co-occurring with them across selected seed species.**

856 Dot plot to indicate co-occurrence of protein families. Black dots in TNP, TIR-only and
857 TNL columns is based on phylogenetic analysis in Figure 1. For all other columns a black
858 dot indicates presence of a protein belonging to that protein orthogroup as identified by
859 Orthofinder, BLASTP or reciprocal tBLASTn.

860

861 **Supplementary Figure 10 *TIR* gene expression in immune-triggered tissues.**

862 Comparison of untriggered and immune-triggered expression of *NLRs* and genes
863 corresponding to conserved *TIR* groups in wild tobacco (*Nicotiana benthamiana*), rice
864 (*Oryza sativa*), maize (*Zea mays*) and the liverwort *Marchantia polymorpha*. Data were
865 taken from publicly available RNAseq experiments including immune-triggered and
866 infected samples. Created with elements from BioRender.com.

867

868

869 **Supplementary Figure 11 Mutant alleles of *M. polymorpha* and *N. benthamiana tnp***
870 **lines.**

871 **A** Representation of CRISPR/Cas9 mutant *tnp* lines in *Marchantia polymorpha*. Two
872 sgRNA sites targeting the single *TNP* gene in *M. polymorpha* are indicated with arrows.
873 Induced mutations are shown as alignments to the WT sequence. The two independent
874 lines represent independent knockouts.

875 **B** CRISPR/Cas9 *tnp* mutant lines in *Nicotiana benthamiana*. One sgRNA site
876 targeting each of the four *TNP* genes in *N. benthamiana* is indicated with arrows. Induced
877 mutations are shown as alignments to the WT sequence. The two independent lines are
878 homozygous quadruple knockouts.

879

880 **Acknowledgements**

881 We thank Jonathan Jones (Sainsbury Laboratory, Norwich UK) for sharing *N. tabacum*
882 *RNAi:EDS1* seeds. This work was supported by the Max-Planck Society (JEP, FL),
883 Deutsche Forschungsgemeinschaft (DFG; German Research Foundation) SFB-1403–
884 414786233 (JEP, DL, OJ, HL), DFG/Agence Nationale de la Recherche Trilateral
885 'RADAR' grant ANR-15-CE20-0016-01 (JEP, JAD), DFG SPP 'DeCrypt' PA-917/8-1 (JEP,
886 CU), Germany's Excellence Strategy CEPLAS (EXC-2048/1, Project 390686111) (JEP)
887 the Biotechnology and Biological Sciences Research Council (BBSRC Doctoral Training
888 Program BB/M011216/1 to ELB.); the EC | European Research Council (grant ERC-2016-
889 STG-716233-MIREDI to KVK). OJ is a member of the International Max-Planck PhD
890 Research School (IMPRS). We also thank Artem Pankin (formerly, MPIPZ) for advice on
891 phylogenetic analyses and the Earlham Institute Scientific Computing group alongside the
892 Norwich BioScience Institutes Partnership Computing infrastructure for Science (CiS)
893 group for access to high performance computing resources.

894

895 ## References

896 **Adlung N, Prochaska H, Thieme S, Banik A, Blüher D, John P, Nagel O, Schulze S, Gantner J, Delker C, et**
897 **al. 2016.** Non-host Resistance Induced by the Xanthomonas Effector XopQ Is Widespread within
898 the Genus Nicotiana and Functionally Depends on EDS1. *Frontiers in Plant Science* **7**: 1796.
899 **Anthoney N, Foldi I, Hidalgo A. 2018.** Toll and Toll-like receptor signalling in development. *Development*
900 **145**(9).
901 **Baggs E, Dagdas G, Krasileva KV. 2017.** NLR diversity, helpers and integrated domains: making sense of
902 the NLR IDentity. *Curr Opin Plant Biol* **38**: 59-67.
903 **Baggs EL, Monroe JG, Thanki AS, O'Grady R, Schudoma C, Haerty W, Krasileva KV. 2020.** Convergent Loss
904 of an EDS1/PAD4 Signaling Pathway in Several Plant Lineages Reveals Coevolved Components of
905 Plant Immunity and Drought Response[OPEN]. *The Plant Cell* **32**(7): 2158-2177.
906 **Bayless AM, Nishimura MT. 2020.** Enzymatic Functions for Toll/Interleukin-1 Receptor Domain Proteins in
907 the Plant Immune System. *Frontiers in Genetics* **11**: 539.
908 **Bernoux M, Ve T, Williams S, Warren C, Hatters D, Valkov E, Zhang X, Ellis JG, Kobe B, Dodds PN. 2011.**
909 Structural and functional analysis of a plant resistance protein TIR domain reveals interfaces for
910 self-association, signaling, and autoregulation. *Cell Host Microbe* **9**(3): 200-211.
911 **Bhandari DD, Lapin D, Kracher B, von Born P, Bautor J, Niefind K, Parker JE. 2019.** An EDS1 heterodimer
912 signalling surface enforces timely reprogramming of immunity genes in Arabidopsis. *Nat Commun*
913 **10**(1): 772.
914 **Bisceglia NG, Gravino M, Savatin DV. 2015.** Luminol-based Assay for Detection of Immunity Elicitor-
915 induced Hydrogen Peroxide Production in Arabidopsis thaliana Leaves. *Bio-protocol* **5**(24): e1685.
916 **Bolger AM, Lohse M, Usadel B. 2014.** Trimmomatic: a flexible trimmer for Illumina sequence data.
917 *Bioinformatics* **30**(15): 2114-2120.
918 **Bowman JL, Kohchi T, Yamato KT, Jenkins J, Shu S, Ishizaki K, Yamaoka S, Nishihama R, Nakamura Y,**
919 **Berger F, et al. 2017.** Insights into Land Plant Evolution Garnered from the Marchantia polymorpha
920 Genome. *Cell* **171**(2): 287-304 e215.
921 **Burdett H, Hu X, Rank MX, Maruta N, Kobe B. 2021.** Self-association configures the NAD⁺-
922 binding site of plant NLR TIR domains. *bioRxiv*: 2021.2010.2002.462850.
923 **Chernomor O, von Haeseler A, Minh BQ. 2016.** Terrace Aware Data Structure for Phylogenomic Inference
924 from Supermatrices. *Syst Biol* **65**(6): 997-1008.
925 **Cirl C, Wieser A, Yadav M, Duerr S, Schubert S, Fischer H, Stappert D, Wantia N, Rodriguez N, Wagner H,**
926 **et al. 2008.** Subversion of Toll-like receptor signaling by a unique family of bacterial
927 Toll/interleukin-1 receptor domain-containing proteins. *Nat Med* **14**(4): 399-406.
928 **Clabbers MTB, Holmes S, Muusse TW, Vajjhala PR, Thygesen SJ, Malde AK, Hunter DJB, Croll TI,**
929 **Flueckiger L, Nanson JD, et al. 2021.** MyD88 TIR domain higher-order assembly interactions
930 revealed by microcrystal electron diffraction and serial femtosecond crystallography. *Nat Commun*
931 **12**(1): 2578.
932 **Coronas-Serna JM, Louche A, Rodríguez-Escudero M, Roussin M, Imbert PRC, Rodríguez-Escudero I,**
933 **Terradot L, Molina M, Gorvel J-P, Cid VJ, et al. 2020.** The TIR-domain containing effectors BtpA
934 and BtpB from Brucella abortus impact NAD metabolism. *PLOS Pathogens* **16**(4): e1007979.
935 **Dongus JA, Parker JE. 2021.** EDS1 signalling: At the nexus of intracellular and surface receptor immunity.
936 *Curr Opin Plant Biol* **62**: 102039.
937 **Duxbury Z, Wang S, MacKenzie CI, Tenthorey JL, Zhang X, Huh SU, Hu L, Hill L, Ngou PM, Ding P, et al.**
938 **2020.** Induced proximity of a TIR signaling domain on a plant-mammalian NLR chimera activates
939 defense in plants. *Proc Natl Acad Sci U S A* **117**(31): 18832-18839.
940 **Eastman S, Smith T, Zaydman MA, Kim P, Martinez S, Damaraju N, DiAntonio A, Milbrandt J, Clemente**
941 **TE, Alfano JR, et al. 2021.** A phytobacterial TIR domain effector manipulates NAD(+) to promote
942 virulence. *New Phytol*.

Essuman K, Summers DW, Sasaki Y, Mao X, DiAntonio A, Milbrandt J. 2017. The SARM1 Toll/Interleukin-1 Receptor Domain Possesses Intrinsic NAD⁺ Cleavage Activity that Promotes Pathological Axonal Degeneration. *Neuron* **93**(6): 1334-1343.e1335.

Essuman K, Summers DW, Sasaki Y, Mao X, Yim AKY, DiAntonio A, Milbrandt J. 2018. TIR Domain Proteins Are an Ancient Family of NAD+-Consuming Enzymes. *Current Biology* **28**(3): 421-430.e424.

Fields JK, Gunther S, Sundberg EJ. 2019. Structural Basis of IL-1 Family Cytokine Signaling. *Front Immunol* **10**: 1412.

Figley MD, Gu W, Nanson JD, Shi Y, Sasaki Y, Cunnea K, Malde AK, Jia X, Luo Z, Saikot FK, et al. 2021. SARM1 is a metabolic sensor activated by an increased NMN/NAD(+) ratio to trigger axon degeneration. *Neuron* **109**(7): 1118-1136 e1111.

Gantner J, Ordon J, Kretschmer C, Guerois R, Stuttmann J. 2019. An EDS1-SAG101 Complex Is Essential for TNL-Mediated Immunity in Nicotiana benthamiana. *The Plant Cell* **31**(10): 2456-2474.

Gao Y, Wang W, Zhang T, Gong Z, Zhao H, Han GZ. 2018. Out of Water: The Origin and Early Diversification of Plant R-Genes. *Plant Physiol* **177**(1): 82-89.

Gerdts J, Brace EJ, Sasaki Y, DiAntonio A, Milbrandt J. 2015. SARM1 activation triggers axon degeneration locally via NAD(+) destruction. *Science* **348**(6233): 453-457.

Horsefield S, Burdett H, Zhang X, Manik MK, Shi Y, Chen J, Qi T, Gilley J, Lai J-S, Rank MX, et al. 2019. NAD+ cleavage activity by animal and plant TIR domains in cell death pathways. *Science* **365**(6455): 793.

Jones JD, Vance RE, Dangl JL. 2016. Intracellular innate immune surveillance devices in plants and animals. *Science* **354**(6316).

Kanduri C, Ukkola-Vuoti L, Oikkonen J, Buck G, Blancher C, Raijas P, Karma K, Lahdesmaki H, Jarvela I. 2013. The genome-wide landscape of copy number variations in the MUSGEN study provides evidence for a founder effect in the isolated Finnish population. *Eur J Hum Genet* **21**(12): 1411-1416.

Katoh K, Misawa K, Kuma K, Miyata T. 2002. MAFFT: a novel method for rapid multiple sequence alignment based on fast Fourier transform. *Nucleic Acids Res* **30**(14): 3059-3066.

Krasileva KV, Dahlbeck D, Staskawicz BJ. 2010. Activation of an Arabidopsis Resistance Protein Is Specified by the in Planta Association of Its Leucine-Rich Repeat Domain with the Cognate Oomycete Effector *The Plant Cell* **22**(7): 2444-2458.

Kubota A, Ishizaki K, Hosaka M, Kohchi T. 2013. Efficient Agrobacterium-mediated transformation of the liverwort Marchantia polymorpha using regenerating thalli. *Biosci Biotechnol Biochem* **77**(1): 167-172.

Kumar S, Stecher G, Suleski M, Hedges SB. 2017. TimeTree: A Resource for Timelines, Timetrees, and Divergence Times. *Mol Biol Evol* **34**(7): 1812-1819.

Lapin D, Bhandari DD, Parker JE. 2020. Origins and Immunity Networking Functions of EDS1 Family Proteins. *Annual Review of Phytopathology* **58**(1): 253-276.

Lapin D, Kovacova V, Sun X, Dongus JA, Bhandari D, von Born P, Bautor J, Guarneri N, Rzemieniewski J, Stuttmann J, et al. 2019. A Coevolved EDS1-SAG101-NRG1 Module Mediates Cell Death Signaling by TIR-Domain Immune Receptors. *The Plant Cell* **31**(10): 2430-2455.

Letunic I, Bork P. 2021. Interactive Tree Of Life (iTOL) v5: an online tool for phylogenetic tree display and annotation. *Nucleic Acids Res* **49**(W1): W293-W296.

Leulier F, Lemaitre B. 2008. Toll-like receptors — taking an evolutionary approach. *Nature Reviews Genetics* **9**(3): 165-178.

Liu Y, Zeng Z, Zhang YM, Li Q, Jiang XM, Jiang Z, Tang JH, Chen D, Wang Q, Chen JQ, et al. 2021. An angiosperm NLR atlas reveals that NLR gene reduction is associated with ecological specialization and signal transduction component deletion. *Mol Plant*.

Ma S, Lapin D, Liu L, Sun Y, Song W, Zhang X, Logemann E, Yu D, Wang J, Jirschitzka J, et al. 2020. Direct pathogen-induced assembly of an NLR immune receptor complex to form a holoenzyme. *Science* **370**(6521): eabe3069.

Martin R, Qi T, Zhang H, Liu F, King M, Toth C, Nogales E, Staskawicz BJ. 2020. Structure of the activated ROQ1 resistosome directly recognizing the pathogen effector XopQ. *Science* **370**(6521): eabd9993.

Meyers BC, Morgante M, Michelmore RW. 2002. TIR-X and TIR-NBS proteins: two new families related to disease resistance TIR-NBS-LRR proteins encoded in Arabidopsis and other plant genomes. *The Plant Journal* **32**(1): 77-92.

Michael TA-O, Ernst EA-OX, Hartwick N, Chu PA-OX, Bryant DA-O, Gilbert SA-O, Ortleb SA-O, Baggs EA-O, Sree KA-O, Appenroth KA-O, et al. 2020. Genome and time-of-day transcriptome of Wolffia australiana link morphological minimization with gene loss and less growth control. *Genome Res.*(1549-5469 (Electronic)).

Morehouse BR, Govande AA, Millman A, Keszei AFA, Lowey B, Ofir G, Shao S, Sorek R, Kranzusch PJ. 2020. STING cyclic dinucleotide sensing originated in bacteria. *Nature* **586**(7829): 429-433.

Nandety RS, Caplan JL, Cavanaugh K, Perroud B, Wroblewski T, Michelmore RW, Meyers BC. 2013. The Role of TIR-NBS and TIR-X Proteins in Plant Basal Defense Responses *Plant Physiology* **162**(3): 1459-1472.

Nanson JD, Rahaman MH, Ve T, Kobe B. 2020. Regulation of signaling by cooperative assembly formation in mammalian innate immunity signalosomes by molecular mimics. *Semin Cell Dev Biol* **99**: 96-114.

Nguyen LT, Schmidt HA, von Haeseler A, Minh BQ. 2015. IQ-TREE: a fast and effective stochastic algorithm for estimating maximum-likelihood phylogenies. *Mol Biol Evol* **32**(1): 268-274.

Nimma S, Ve T, Williams SJ, Kobe B. 2017. Towards the structure of the TIR-domain signalosome. *Current Opinion in Structural Biology* **43**: 122-130.

Nishimura MT, Anderson RG, Cherkis KA, Law TF, Liu QL, Machius M, Nimchuk ZL, Yang L, Chung E-H, El Kasmi F, et al. 2017. TIR-only protein RBA1 recognizes a pathogen effector to regulate cell death in <em>Arabidopsis</em&gt. *Proceedings of the National Academy of Sciences* **114**(10): E2053.

Nozawa M, Nei M. 2008. Genomic drift and copy number variation of chemosensory receptor genes in humans and mice. *Cytogenet Genome Res* **123**(1-4): 263-269.

O'Neill LAJ, Bowie AG. 2007. The family of five: TIR-domain-containing adaptors in Toll-like receptor signalling. *Nature Reviews Immunology* **7**(5): 353-364.

Ofir G, Herbst E, Baroz M, Cohen D, Millman A, Doron S, Tal N, Malheiro DBA, Malitsky S, Amitai G, et al. 2021. Antiviral activity of bacterial TIR domains via signaling molecules that trigger cell death. *bioRxiv*: 2021.2001.2006.425286.

Patro R, Duggal G, Love MI, Irizarry RA, Kingsford C. 2017. Salmon provides fast and bias-aware quantification of transcript expression. *Nat Methods* **14**(4): 417-419.

Prigozhin DM, Krasileva KV. 2021. Analysis of intraspecies diversity reveals a subset of highly variable plant immune receptors and predicts their binding sites. *Plant Cell* **33**(4): 998-1015.

Saile SC, Jacob P, Castel B, Jubic LM, Salas-Gonzáles I, Bäcker M, Jones JDG, Dangl JL, El Kasmi F. 2020. Two unequally redundant "helper" immune receptor families mediate Arabidopsis thaliana intracellular "sensor" immune receptor functions. *PLOS Biology* **18**(9): e3000783.

Saucet SB, Esmenjaud D, Van Ghelder C. 2021. Integrity of the Post-LRR Domain Is Required for TIR-NB-LRR Function. *Mol Plant Microbe Interact* **34**(3): 286-296.

Schultink A, Qi T, Lee A, Steinbrenner AD, Staskawicz B. 2017. Roq1 mediates recognition of the Xanthomonas and Pseudomonas effector proteins XopQ and HopQ1. *The Plant Journal* **92**(5): 787-795.

Shao Z-Q, Xue J-Y, Wu P, Zhang Y-M, Wu Y, Hang Y-Y, Wang B, Chen J-Q. 2016. Large-Scale Analyses of Angiosperm Nucleotide-Binding Site-Leucine-Rich Repeat Genes Reveal Three Anciently Diverged Classes with Distinct Evolutionary Patterns. *Plant Physiology* **170**(4): 2095-2109.

1039 **Shao ZQ, Xue JY, Wang Q, Wang B, Chen JQ. 2019.** Revisiting the Origin of Plant NBS-LRR Genes. *Trends*
1040 *Plant Sci* **24**(1): 9-12.
1041 **Sohn KH, Segonzac C, Rallapalli G, Sarris PF, Woo JY, Williams SJ, Newman TE, Paek KH, Kobe B, Jones**
1042 **JD. 2014.** The nuclear immune receptor RPS4 is required for RRS1SLH1-dependent constitutive
1043 defense activation in Arabidopsis thaliana. *PLoS Genet* **10**(10): e1004655.
1044 **Soneson C, Love MI, Robinson MD. 2015.** Differential analyses for RNA-seq: transcript-level estimates
1045 improve gene-level inferences. *F1000Res* **4**: 1521.
1046 **Sporny M, Guez-Haddad J, Lebendiker M, Ulisse V, Volf A, Mim C, Isupov MN, Opatowsky Y. 2019.**
1047 Structural Evidence for an Octameric Ring Arrangement of SARM1. *J Mol Biol* **431**(19): 3591-3605.
1048 **Steuernagel B, Witek K, Krattinger SG, Ramirez-Gonzalez RH, Schoonbeek HJ, Yu G, Baggs E, Witek AI,**
1049 **Yadav I, Krasileva KV, et al. 2020.** The NLR-Annotator Tool Enables Annotation of the Intracellular
1050 Immune Receptor Repertoire. *Plant Physiol* **183**(2): 468-482.
1051 **Sun X, Lapin D, Feehan JM, Stolze SC, Kramer K, Dongus JA, Rzemieniewski J, Blanvillain-Baufume S,**
1052 **Harzen A, Bautor J, et al. 2021.** Pathogen effector recognition-dependent association of NRG1
1053 with EDS1 and SAG101 in TNL receptor immunity. *Nat Commun* **12**(1): 3335.
1054 **Sun X, Pang H, Li M, Chen J, Hang Y. 2014.** Tracing the origin and evolution of plant TIR-encoding genes.
1055 *Gene* **546**(2): 408-416.
1056 **Tamborski J, Krasileva KV. 2020.** Evolution of Plant NLRs: From Natural History to Precise Modifications.
1057 *Annual Review of Plant Biology* **71**(1): 355-378.
1058 **Tian H, Wu Z, Chen S, Ao K, Huang W, Yaghmaiean H, Sun T, Xu F, Zhang Y, Wang S, et al. 2021.** Activation
1059 of TIR signalling boosts pattern-triggered immunity. *Nature* **598**(7881): 500-503.
1060 **Toshchakov VY, Neuwald AF. 2020.** A survey of TIR domain sequence and structure divergence.
1061 *Immunogenetics* **72**(3): 181-203.
1062 **Van Ghelder C, Esmenjaud D. 2016.** TNL genes in peach: insights into the post-LRR domain. *BMC Genomics*
1063 **17**: 317.
1064 **Wagner S, Stuttmann J, Rietz S, Guerois R, Brunstein E, Bautor J, Niefind K, Parker Jane E. 2013.** Structural
1065 Basis for Signaling by Exclusive EDS1 Heteromeric Complexes with SAG101 or PAD4 in Plant Innate
1066 Immunity. *Cell Host & Microbe* **14**(6): 619-630.
1067 **Wan L, Essuman K, Anderson RG, Sasaki Y, Monteiro F, Chung E-H, Osborne Nishimura E, DiAntonio A,**
1068 **Milbrandt J, Dangl JL, et al. 2019.** TIR domains of plant immune receptors are
1069 NAD⁺-cleaving enzymes that promote cell death. *Science* **365**(6455): 799.
1070 **Williams SJ, Sohn KH, Wan L, Bernoux M, Sarris PF, Segonzac C, Ve T, Ma Y, Saucet SB, Ericsson DJ, et al.**
1071 **2014.** Structural Basis for Assembly and Function of a Heterodimeric Plant Immune Receptor.
1072 *Science* **344**(6181): 299.
1073 **Witte CP, Noel LD, Gielbert J, Parker JE, Romeis T. 2004.** Rapid one-step protein purification from plant
1074 material using the eight-amino acid StrepII epitope. *Plant Mol Biol* **55**(1): 135-147.
1075 **Yadav M, Zhang J, Fischer H, Huang W, Lutay N, Cirl C, Lum J, Miethke T, Svanborg C. 2010.** Inhibition of
1076 TIR domain signaling by TcpC: MyD88-dependent and independent effects on Escherichia coli
1077 virulence. *PLoS Pathog* **6**(9): e1001120.
1078 **Yu D, Song W, Tan EYJ, Liu L, Cao Y, Jirschitzka J, Li E, Logemann E, Xu C, Huang S, et al. 2021.** TIR domains
1079 of plant immune receptors are 2′,3′-cAMP/cGMP synthetases mediating cell death. *bioRxiv*:
1080 2021.2011.2009.467869.
1081 **Yu G. 2020.** Using ggtree to Visualize Data on Tree-Like Structures. *Curr Protoc Bioinformatics* **69**(1): e96.
1082 **Zhang X, Bernoux M, Bentham AR, Newman TE, Ve T, Casey LW, Raaymakers TM, Hu J, Croll TI, Schreiber**
1083 **KJ, et al. 2017a.** Multiple functional self-association interfaces in plant TIR domains. *Proceedings*
1084 *of the National Academy of Sciences* **114**(10): E2046.
1085 **Zhang X, Dodds PN, Bernoux M. 2017b.** What Do We Know About NOD-Like Receptors in Plant Immunity?
1086 *Annual Review of Phytopathology* **55**(1): 205-229.

1087 **Zhang Y-M, Xue J-Y, Liu L-W, Sun X-Q, Zhou G-C, Chen M, Shao Z-Q, Hang Y-Y. 2017.** Divergence and
1088 Conservative Evolution of XTNX Genes in Land Plants. *Frontiers in Plant Science* **8**: 1844.
1089 **Zhang Y, Xia R, Kuang H, Meyers BC. 2016.** The Diversification of Plant NBS-LRR Defense Genes Directs the
1090 Evolution of MicroRNAs That Target Them. *Molecular Biology and Evolution* **33**(10): 2692-2705.
1091 **Zhao T, Zwaenepoel A, Xue JY, Kao SM, Li Z, Schranz ME, Van de Peer Y. 2021.** Whole-genome
1092 microsynteny-based phylogeny of angiosperms. *Nat Commun* **12**(1): 3498.

1093